INL/EXT-11-23265
Revision 1

Tritium Permeability of Incoloy 800H and Inconel 617

Paul Humrickhouse, Robert Pawelko, Masashi Shimada, and Philip Winston

July 2012

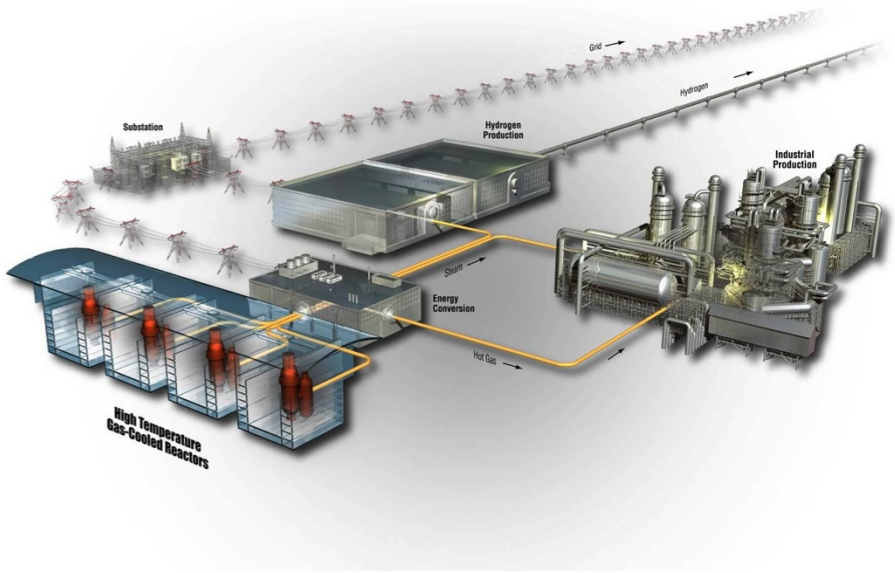

The INL is a
U.S. Department of Energy
National Laboratory
operated by
Battelle Energy Alliance

Idaho National Laboratory

INL/EXT-11-23265
Revision 1

Tritium Permeability of Incoloy 800H and Inconel 617

**Paul Humrickhouse, Robert Pawelko,
Masashi Shimada, and Philip Winston**

July 2012

**Idaho National Laboratory
Very High Temperature Reactor Program
Idaho Falls, Idaho 83415**

http://www.inl.gov

**Prepared for the
U.S. Department of Energy
Office of Nuclear Energy
Under DOE Idaho Operations Office
Contract DE-AC07-05ID14517**

Very High Temperature Reactor Program

Tritium Permeability of Incoloy 800H and Inconel 617

INL/EXT-11-23265
Revision 1

July 2012

Prepared by:

P. Humrickhouse — Date: 6-21-12

Approved by:

P. Winston — Date: 7-10-12

M. Shimada (MASASHI SHIMADA by Phillip Winston) — Date: 7-10-12

J. Simonds — Date: 7/11/2012
Project Manager, AGR Fuel Development Program

K. J. Armour (for) — Date: 7/12/12
Very High Temperature Reactor Quality Assurance Lead

D. A. Petti (for) — Date: 7/12/12
Very High Temperature Reactor Technology
Development Office

ABSTRACT

Design of the Next Generation Nuclear Plant (NGNP) reactor and its high-temperature components requires information regarding the permeation of fission generated tritium and hydrogen product through candidate heat exchanger alloys. Release of fission-generated tritium to the environment and the potential contamination of the helium coolant by permeation of product hydrogen into the coolant system represent safety basis and product contamination issues. Of the three potential candidates for high-temperature components of the NGNP reactor design, only permeability for Incoloy 800H has been well documented.

To support engineering design of the NGNP reactor components, tritium permeability values for Inconel 617 and Incoloy 800H were determined in Fiscal Year 2011 using a measurement system designed and fabricated at Idaho National Laboratory. The measured tritium permeability of Incoloy 800H and Inconel 617 deviated substantially from the values measured for hydrogen. The experiments were repeated in FY-12 with Incoloy 800H using reconfigured tritium detection and in-process hydrogen measurement to reduce uncertainties from the first series of tests. The tritium permeability of Incoloy 800H was measured in the temperature range 700 to 950°C and at primary concentrations of 0.5 to 125 (atom) parts per million tritium in helium (partial pressures of 10^{-7} atm) - four orders of magnitude lower partial pressure than used in the hydrogen permeation testing. The new data provide some evidence that permeation has become surface-limited, as expected for sufficiently low pressures. In this case, the resultant tritium flux is linearly related to the pressure, unlike the diffusion-limited (high pressure) regime, in which it is proportional to the square root of pressure. In the surface-limited regime, the proportionality constant is not the permeability K, but the dissociation rate constant K_d. Since the present measurements appear to span at least a part of the transition region between these two extremes, a quantitative estimate of K_d could not be obtained, but the theory and experimental requirements for doing so are outlined.

ACKNOWLEDGEMENTS

This report builds on work done during FY-10 by Pattrick Calderoni and Matthias Ebner. Various description sections are derived from report number INL/EXT-10-19387, Hydrogen Permeability of Incoloy 800H, Inconel 617 and Haynes 230.

CONTENTS

FIGURES

TABLES

ACRONYMS

CPM	compact process monitor
DU	depleted uranium
FY	Fiscal year
HT	hydrogen-tritium
NGNP	Next Generation Nuclear Plant
ppma	atom parts-per-million
SAS	Tritium Storage and Assay System
SEM	scanning electron microscopy
sscm	standard cubic centimeters per minute
STAR	Safety and Tritium Applied Research Facility
TMIST	Tritium Migration, Infiltration, and Scintillation Test
UHP	ultra high purity
VHTR	very high temperature reactor

Tritium Permeability of Incoloy 800H and Inconel 617

1. INTRODUCTION

The U.S. Department of Energy has selected the very high temperature reactor (VHTR) concept for the Next Generation Nuclear Plant (NGNP). Conceptually, the NGNP can produce electricity, generate hydrogen, and provide industrial process heat at temperatures up to 950°C. The NGNP conceptual design is a graphite reactor core with a helium primary coolant. The very high outlet temperatures impose severe service requirements on the structural components of the reactor and intermediate heat exchanger. The need for resistance to high temperature creep severely limits candidate metals to high-nickel alloys. Alloys that are candidates for high-temperature structural components are Incoloy 800H, Inconel 617, and Haynes 230 [1].

Containment of fission products is a paramount concern in the operation of a nuclear reactor. The safety basis requires information regarding the release characteristics of the materials chosen for the reactor and process components. The containment of fission product tritium is of special concern in the NGNP because of its mobility in the core at the high operating temperatures. Tritium is a radioactive isotope of hydrogen. As an internal radiological hazard to humans, it has stringent federal release limits. Because of its mobility at the design reactor outlet temperatures, tritium can permeate through the walls of the intermediate heat exchanger and steam generator systems, potentially contaminating the environment and the hydrogen product. Tritium will be produced in the reactor as a ternary fission product. It is also produced by activation of graphite contaminants such as lithium (Li-6 and Li-7); of the naturally occurring helium isotope, He-3 in the primary coolant; and the boron in the B_4C burnable neutron poison.

The degree of tritium containment of the NGNP intermediate heat exchanger and the steam generator depends on the selection of materials that allow the control of fission product permeation. Most gases, including hydrogen and tritium, have a finite permeation rate that generally increases exponentially with temperature. The magnitude of the permeation rate may be limited by surface effects or bulk diffusion, which are characteristics determined by the elemental composition, phase composition, microstructure, and surface coatings of the alloys and materials.

The permeation of hydrogen through the candidate alloys was investigated during fiscal year (FY)-10, and permeation of tritium in FY-11 and FY-12. Of the three candidate high-nickel alloys, only Incoloy 800/800H has been significantly tested for permeation, with several reports in the literature as shown in Figure 1 [2-10]. Only two groups have reported hydrogen permeability data for Inconel 617 [5,7]; likewise, two groups have reported tritium permeation for Incoloy 800/800H. The activation energy for diffusion-limited hydrogen permeation, Q (in units of kcal/mol), and the Arrhenius pre-exponential term, K_0 (in units of cm^3 [standard temperature and pressure (STP; 0°C, 1 atmosphere)] hydrogen/cm·sec·$atm^{1/2}$)[a] are given in Table 1 for Incoloy 800/800H and Inconel 617, along with the applicable temperature and pressure ranges for the literature data. With the exception of Roehrig et al. [4], the literature data pertain to hydrogen partial pressures greater than 0.1 atm. All are at substantially higher hydrogen and tritium pressures than are expected to be typical of the steady-state conditions within a VHTR. Different permeation mechanisms may apply at those lower partial pressures. These data must be generated experimentally to support the design of the NGNP systems.

a These units were chosen for ease of comparison with literature data that also use them. To convert to mol/(m•s•$Pa^{1/2}$), divide by 7.66e4.

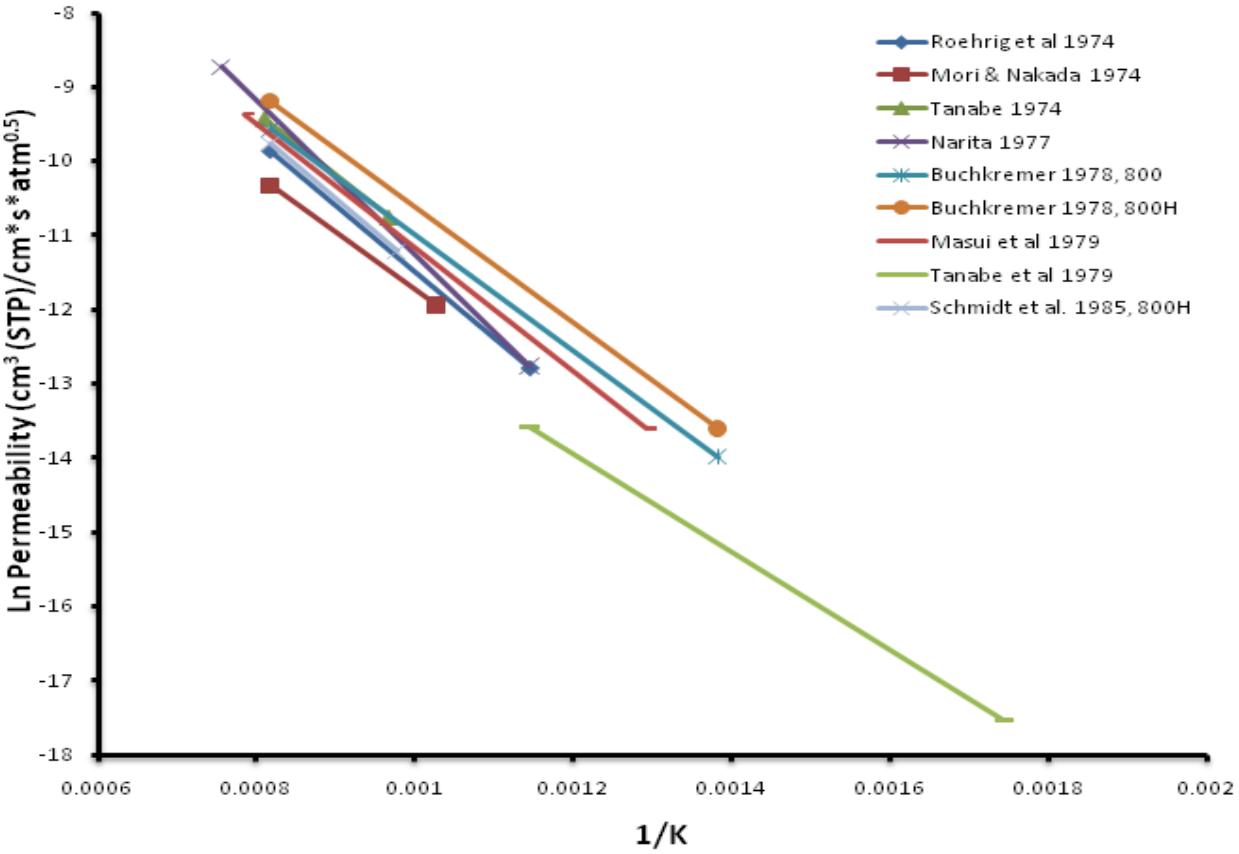

Figure 1. Summary of literature data for hydrogen permeability through Incoloy 800/800H.

Table 1. Literature values of the Arrhenius pre-exponential and activation energy for hydrogen permeation through Incoloy 800/800H, Inconel 617, and Haynes 230.

K_0 cm^3 H_2 (STP)/cm·sec·$atm^{1/2}$	Q kcal/mol	Temp. Range °C	Pressure Range atm	References
Incoloy 800, Hydrogen Permeability				
3.59×10^{-1} *	21.6	650–950	0.001–0.01	[11]
7.39×10^{-2}	17.7	600–950	5×10^{-4} – 0.5	[4]
1.76×10^{-2}	15.3	700–950	1–5	[2]
7.58×10^{-2}	16.8	760–960	1	[8]
4.03×10^{-1}	20.6	600–1050	1–10	[7]
4.02×10^{-2}	15.5	450–950	5–10	[9,12]
5.90×10^{-2} *	15.5 *	450–950	5–10	[9,12]
6.02×10^{-2}	16.6	500–1000	0.1–1	[3]
2.44×10^{-3}	13.1	300–600	0.13–0.8	[6]
9.24×10^{-2} *	18.0 *	750–950	<40	[5]
Incoloy 800, Tritium Permeability				
2.60×10^{-2}	16.1	350–750	2 ppm ^3H, 1 atm H_2	[13,14]
1.50×10^{-3}	13.5	750–950	1×10^{-4}	[5]
Inconel 617, Hydrogen Permeability				
5.39×10^{-1}	21.3	650–950	0.001–0.01	[11]
2.28×10^{-1}	18.9	600–1050	1–10	[7]
1.39×10^{-1}	19.8	750–950	<40	[5]
Haynes 230, Hydrogen Permeability				
No reports	No reports			

* Data for Incoloy 800H

2. OBJECTIVES OF THE RESEARCH

The objective of this work is to experimentally determine the permeation rates of tritium through the candidate alloys for NGNP structural components, which include Incoloy 800H, Inconel 617, and Haynes 230. During FY-2011, only Incoloy 800H and Inconel 617 were tested with tritium.

The work consisted of three phases: (1) acquisition and transfer of a specific quantity of tritium gas into the tritium permeation glove box; (2) determination of the tritium permeation flux through the two candidate alloys at low partial pressures; and (3) determination of the tritium permeation constants from that data. The permeability measurement system was designed for operation with hydrogen or tritium, either as a single-pass or as a recirculation system, and operating at temperatures in the range 700 to 950 °C. Due to limited availability of tritium-helium primary loop gas, the system was operated in a recirculation mode with a fractional bleed off to allow a continuous input. The system was used in FY-10 to test the hydrogen permeability of Incoloy 800H, Inconel 617 and Haynes 230. The tritium permeability of Incoloy 800H and Inconel 617 was measured in the range 650 to 950°C in FY-11. Improved measurments were made in FY-12 at concentrations varying from 0.5 to 125 atom parts-per-million (ppma) tritium in helium.

The initial version of this report summarizes the measurement of tritium permeability at high temperatures through the two candidate alloys. Revision 1 addresses the observation from the first round of tests that the permeability was reduced at low partial pressures by more than two orders of magnitude compared to previous hydrogen tests. This is significant for calculation of expected tritium releases in the reactor source term. The VHTR is expected to have tritium concentrations similar to the low range of values tested here.

3. DESCRIPTION OF THE MEASUREMENT SYSTEM, SAMPLES, AND TEST PARAMETERS

3.1 Permeation Measurement System

The measurement system, shown in the simplified diagram in Figure 2(a) and the detailed diagrams in Figure 2(b) and 2(c), consists of two counter-flowing gas flow loops separated by the heated tubular test sample. The thin-walled tubular sample, mounted inside a sealed quartz sample chamber, is the permeation interface separating the primary and secondary gas loops. The helium-tritium test gas mixture in the primary gas loop flows through the bore of the tubular test sample, while the helium of the secondary gas loop flows over the external surface of the tubular sample. The concentration of the permeated hydrogen gas in the helium of the secondary gas loop was measured by a quadrupole mass spectrometer and, in the tritium measurements, by an ion chamber.

The permeation measurement system is a sealed system housed in a glove box, as shown in Figure 3, for contamination control during tritium testing. The gas exhausted from the experiment glovebox is transferred to the tritium recovery ventilation hood prior to venting to the stack. The system was fabricated with 316 and 304 stainless steel components, tubing, and welded compression fittings (component sources for the measurement system are listed in Table 2). The vacuum integrity of the system was confirmed at a leak rate of less than 10^{-5} std. cc/sec by helium leak testing. The system had provisions for introduction of gas mixtures used for the permeation probe mixture in the primary loop, introduction of ultra-high purity helium for the sweep gas in the secondary loop, getter modules for purification of the helium gas streams, a rotary pump and turbomolecular vacuum pump for evacuation and clean up of the gas loops, and metal bellows pumps for the circulation of the gas flows in the loops.

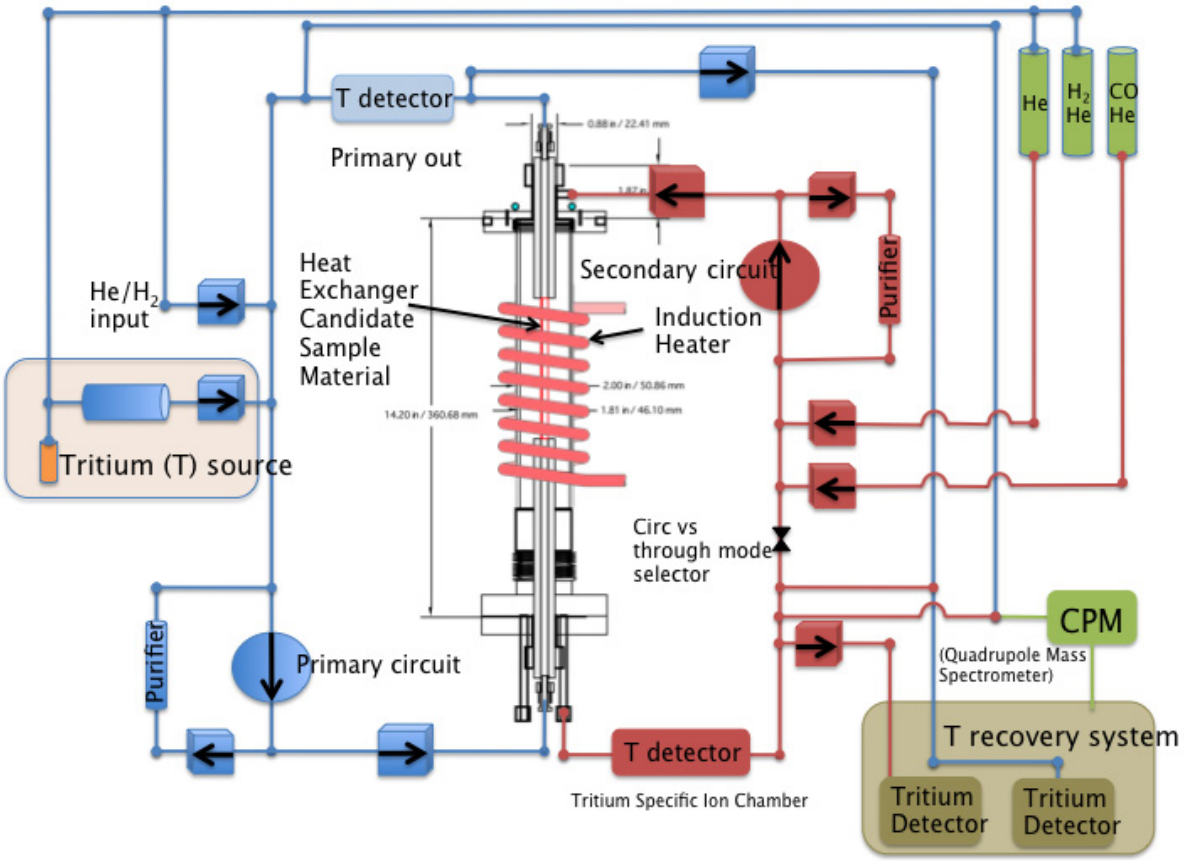

Figure 2(a). Simplified diagram of the permeability measurement system.

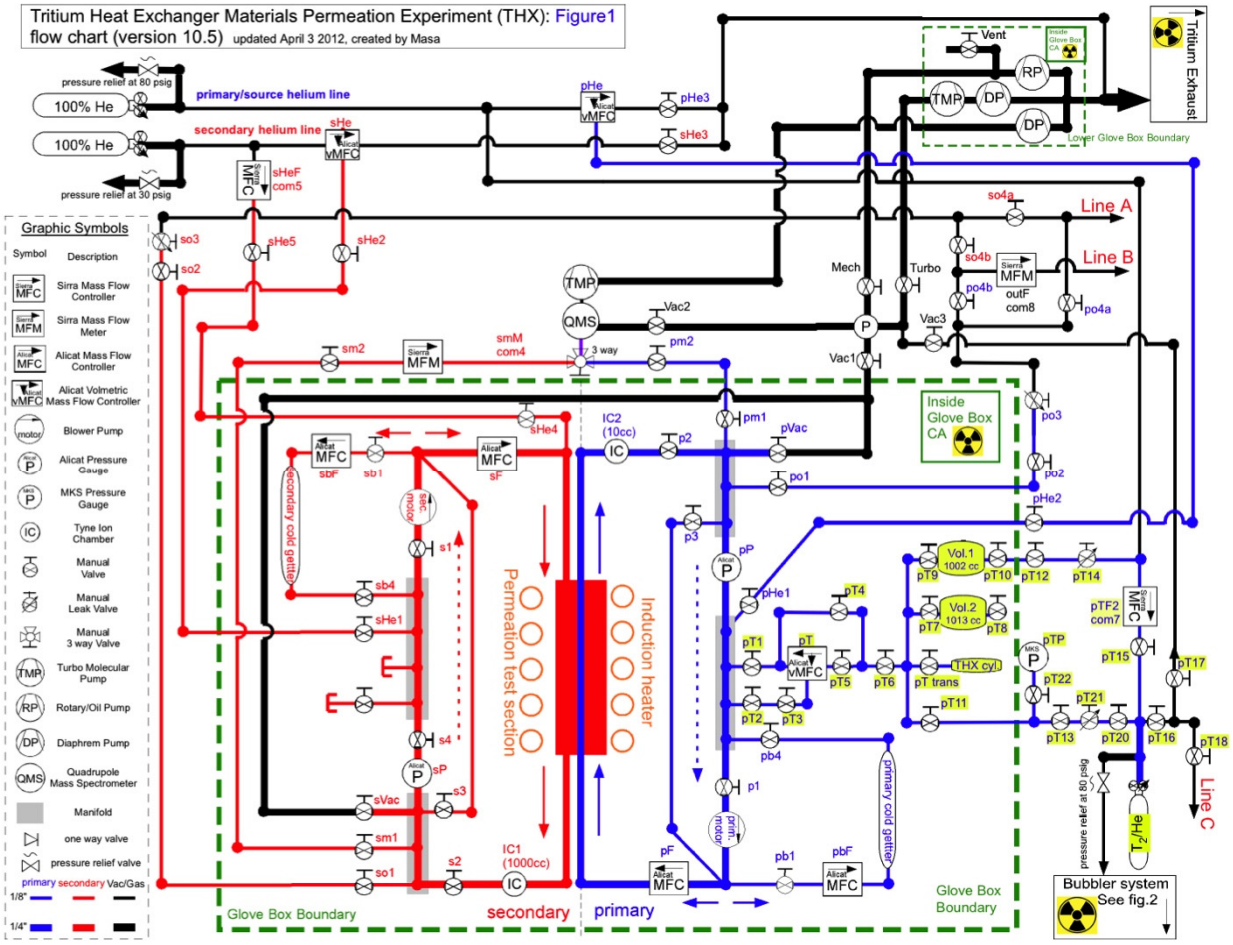

Figure 2(b). Detailed diagram of the permeability measurement system inside the glove box.

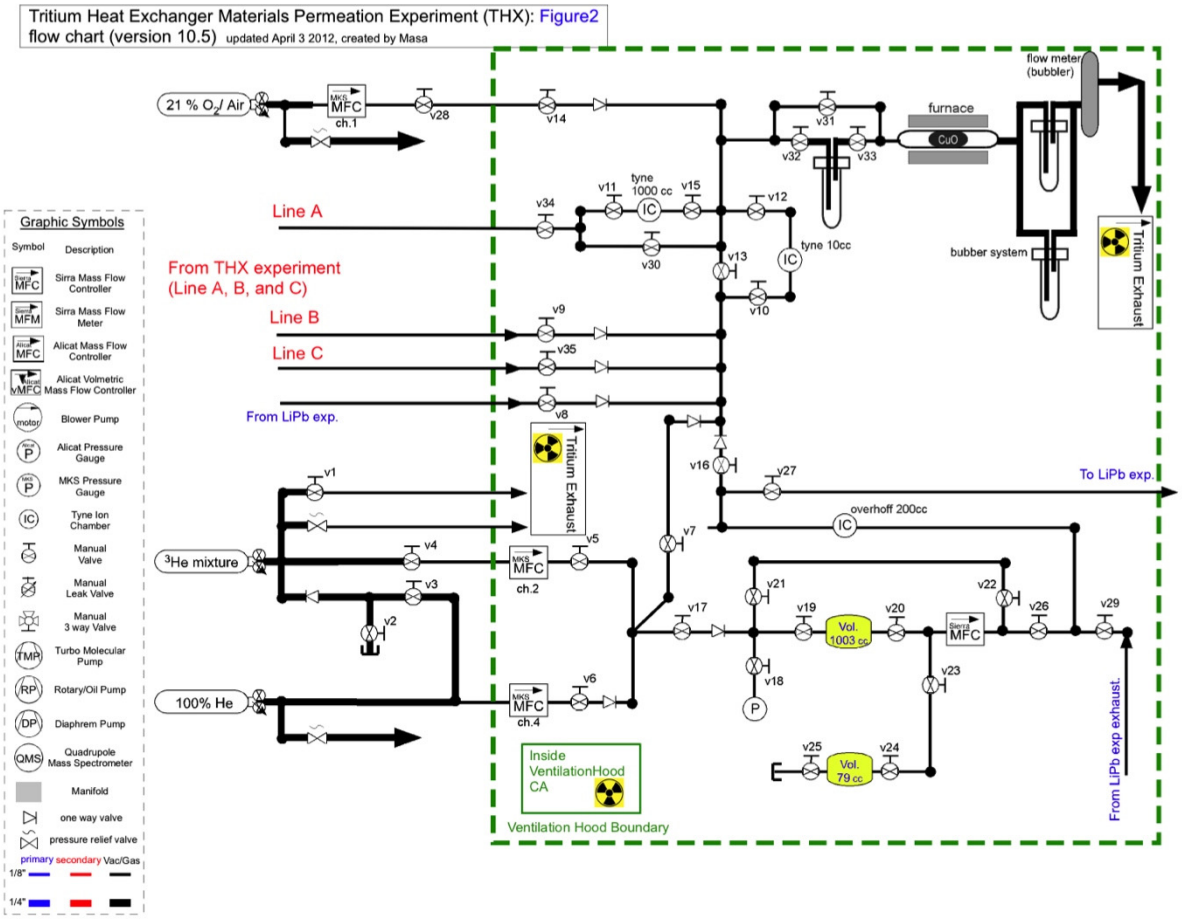

Figure 2(c). Detailed diagram of the permeability measurement system inside the ventilation hood.

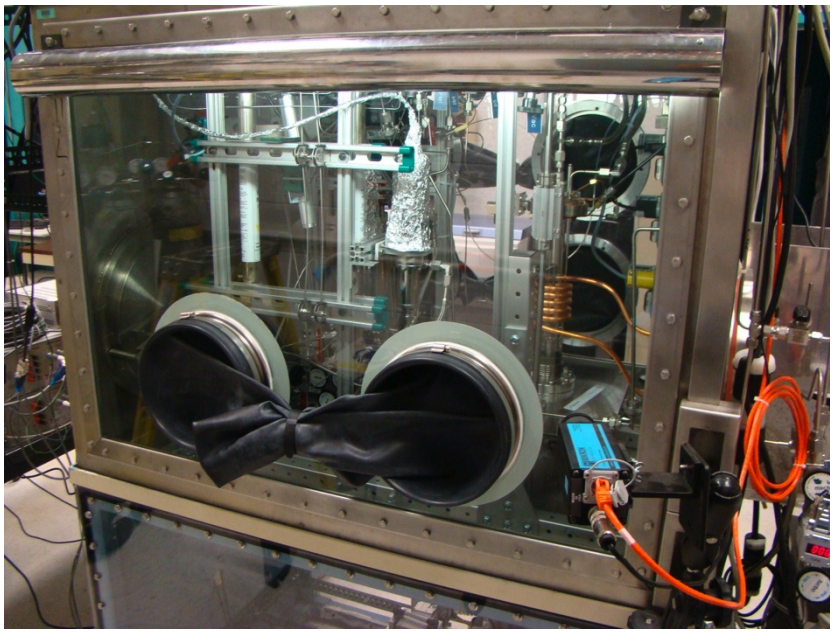

Figure 3. The permeability measurement system assembled within a glove box for work with tritium permeation. Infrared camera is visible connected to orange cable.

Table 2. Sources of components.

Component	Item	Model	Manufacturer
Compression fittings		VCR	Swagelok, Inc.
Purification getters		HP-2, P100-2	VICI Valco Instruments Company, Inc
Rotary pump		RV5	Edwards, Inc.
Turbomolecular pump		TMH 071P	Pfeiffer Vacuum, Inc.
Metal bellows pumps		Model MB-158	Senior Operations, Inc.
Pressure controller	Transducer	PCD-30PSIA-D-25VCRM/5P	Alicat Scientific, Inc.
	Software	Flow Vision™ SC	Alicat Scientific, Inc.
Mass flow controllers	Transducer	MC-10SLPM-D-30PSIA-25VCRM	Alicat Scientific, Inc.
	Software	Flow Vision™ SC	Alicat Scientific, Inc.
	Transducer	C-100L-DD-8-OV1-PV2-V1-SI-CN	Sierra Instruments, Inc.
	Software	Smart-Trak 2™	Sierra Instruments, Inc.
Process control software		LabVIEW, version 8.5.1	National Instruments, Inc.
Mass spectrometer	Spectrometer	Transpector CPM Compact Process Monitor	Inficon, Inc.
	Software	TWare32™	Inficon, Inc.
Sample chamber			Larsen Glass, Inc.
Induction heater		SI-10KWHF	Superior Induction Co.
Control thermocouple	Type K thermocouple		Omega, Inc.
	Read out unit	SXCI-1000	National Instruments, Inc.
Thermal imaging system	Infrared camera	M9200	Mikron Infrared, Inc.
	Software	MikroSpec R/T™ 9200, version 3.9200.117,	Mikron Infrared, Inc.
Alloys for samples	Incoloy 800H, Inconel 617, and Haynes 230		Century Tubes, Inc.
Sample supports	Inconel 600 tubes		TW Metals, Inc.
Gas mixtures	Nominal 1.5, 3, and 6 ppmv tritium in He		INL supplied.
Tritium ion chamber detector	Multi Range Tritium Controller	7000-TC-002-C	Tyne Engineering Inc.
Ion chamber calibration hardware and software for response testing of 10 and 1000 cc ion chambers	7500-MKIT-001-C software, Calibration Procedure, Calibrated voltage-current simulator with certification, Calibrated DMM with certification	Calibration Kit 7000	Tyne Engineering, Inc.

The system is instrumented with pressure and mass flow controllers. The pressure and mass flow controllers operate through a LabVIEW process control software interface. The initial activity of the input gas mixtures in the primary loop was measured using the Tyne ion chamber unit located in the tritium recovery hood adjacent to the permeation system glove box. The output gas in the secondary loop was measured by the Tyne ion chamber units mounted in the glove box. The flow composition of the primary and secondary can alternately be measured using the in-line quadrupole mass spectrometer compact process monitor (CPM), which is capable of sampling gas streams at 1 atm pressure, or using in-line ion chambers for tritium detection. Because the CPM is mounted outside the glove box, it is not considered best practice to run a tritiated gas flow through it. The tritium (and potential hydrogen) gas concentrations are expected to be below its 20 ppmv detection limit, and as such it may not be possible to determine low hydrogen background or distinguish hydrogen-tritium (HT) at mass 4 from helium (mass 4) carrier gas by monitoring with the CPM.

In 2011, detection of tritium diffusing into the secondary chamber was done using a Tyne Engineering Model 7000-TC-002-C ion chamber system that is designed explicitly for detection of tritium. This is a multirange system with two ion chambers in series, one with a 10 cc volume, and the other with a 1000 cc volume. The small chamber provides a rapid response, while the larger chamber gives a high sensitivity for low concentrations. Operationally, the test endpoint was determined to be the time when the two ion chambers showed essentially the same concentrations.

For testing in 2012, the series arrangement of the ion chambers was modified so that the 10 cc ion chamber measured the tritium concentration in the primary (downstream of the sample), and the 1000 cc ion chamber measured the stream in the secondary loop. To further validate the measurements, the primary stream was monitored in the tritium recovery hood using a 1000 cc ion chamber also. In the 2011 tests, the gas flows of the primary and secondary were mixed as they exited the experiment glovebox, prior to flowing through the ion chambers, resulting in an uncertain value for the gas being vented from the primary loop. To measure the prevailing hydrogen background, the quadrupole mass spectrometer was valved in at a point when the secondary loop tritium concentration had reached an apparent equilibrium.

The sample chamber consists of a quartz tube sealed to Kovar transitions between two vacuum flanges, as shown in Figures 2 and 4. The test sample is mounted in the upper and lower vacuum flange by compression O-ring seals, and has VCR gas compression fittings for connection to the primary loop. In this design, the two helium loops sweep the sample chamber in counter-flow manner, with the tritium-helium test gas mixture passing upwards through the bore of the tubular sample, and the helium sweep of the secondary loop flowing downwards through the main chamber volume.

The test sample is heated by a radio frequency induction heater, through the copper coils that surround the quartz chamber, as shown in Figure 4. The induction heater is a water-cooled, 440 Vac, 100 to 300 kHz, 10 kW system. The induction heater is controlled by the National Instruments LabVIEW process control software interface, using a contact thermocouple that is located at the center (midplane) of the heated area of the test sample.

The temperature of the heated area of the test sample is monitored by an infrared thermal imaging system mounted external to the glove box. The system yields two-dimensional (2D) maps of the temperatures of the heated sample area visible in the gaps between the radio frequency heater coils. The system has four temperature ranges that span 600 to 1600°C, with spectral response from 800 to 900 nanometers and temperature resolution of 0.5% of the reading. The thermal imaging system is calibrated against the control thermocouple, allowing evaluation of the emissivity of the sample. Figure 5 shows five regions of interest (oblong boxes) that correspond to a heated sample visible between the induction coil windings, two lines along which the continuous temperature distribution is recorded, and a tabulation of minimum, maximum, and average temperatures for each region or line of interest.

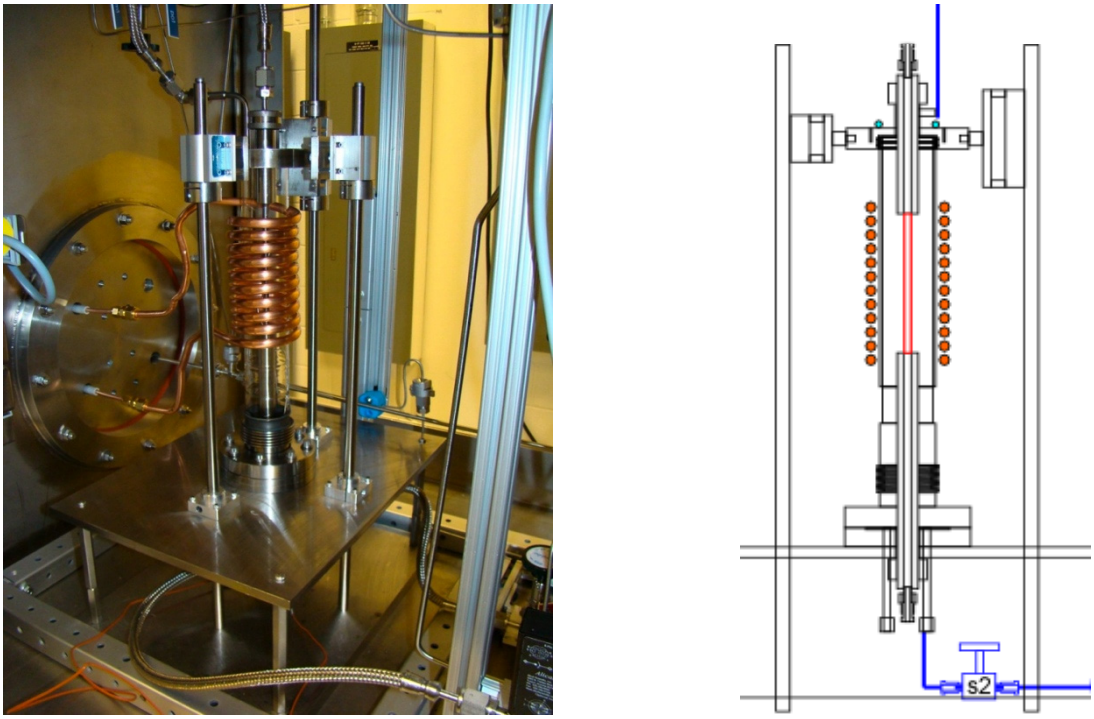

Figure 4. Configuration of the test sample. The picture and drawing show the configuration of the test sample within the quartz-walled test chamber, surrounded by the induction heater coils.

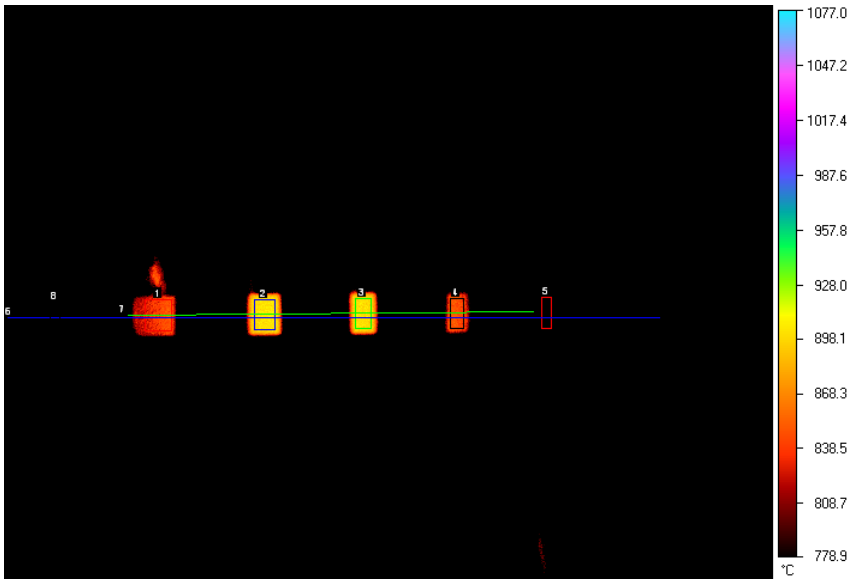

	Min. °C	Max. °C	Avg. °C	Range °C
Rectangle 1	810.1	861.5	839.1	51.4
Rectangle 2	889.0	914.0	902.2	25.0
Rectangle 3	887.3	912.2	900.2	24.9
Rectangle 4	826.3	862.6	846.9	36.3
Rectangle 5	UNDER	769.0	735.6	
Line 6	UNDER	909.7	UNDER	
Line 7	UNDER	911.1	703.0	
Rectangle 8	UNDER	741.0	UNDER	

Figure 5. Sample output of the thermal imaging system.

Data along line 6 of Figure 5 are used to fit a continuous temperature distribution that is used in the permeability analysis. The analytical solution for 1D heat conduction with fixed end temperatures and constant heat generation is quadratic; the data were well fit with this form. The measured and fitted temperature profiles for Incoloy 800H are shown in Figure 6 and for Inconel 617 in Figure 7.

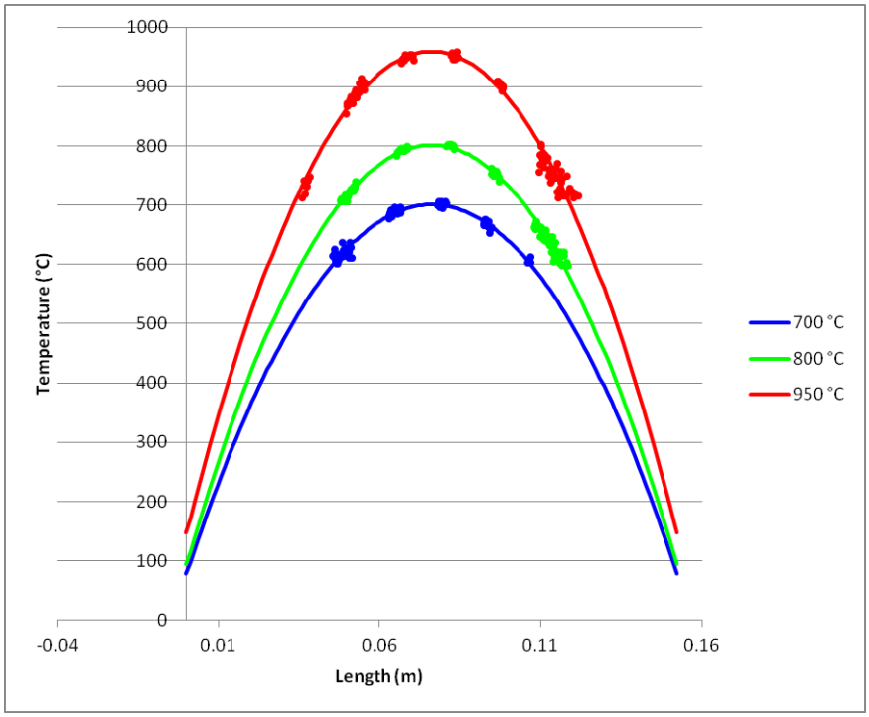

Figure 6. Incoloy 800H axial temperature distribution data and quadratic fit.

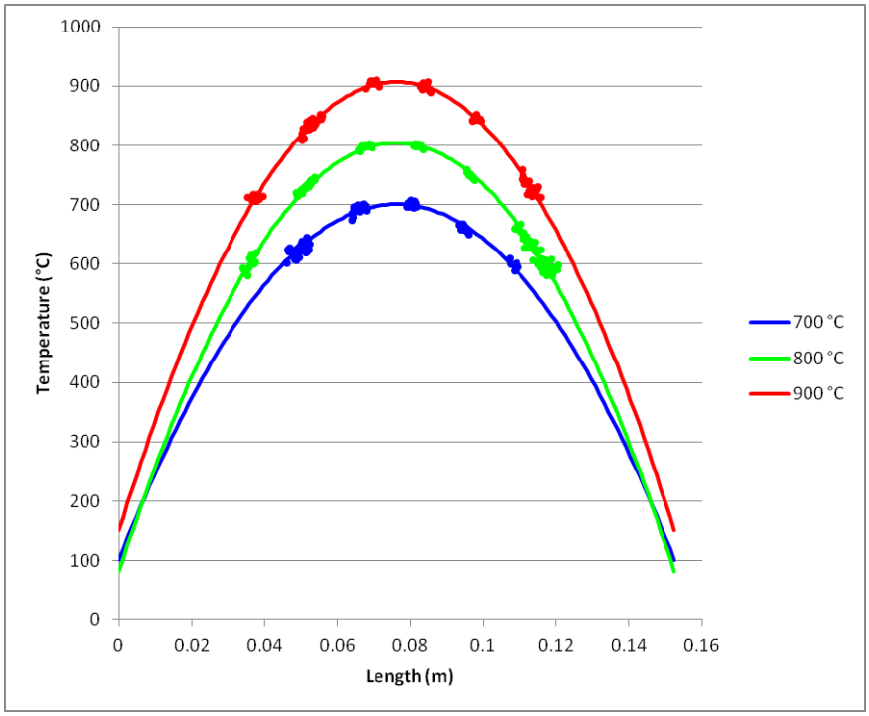

Figure 7. Incoloy 800H axial temperature distribution data and quadratic fit.

3.2 Test Samples

The alloys tested for hydrogen isotope permeability were Incoloy 800H and Inconel 617. The composition of the alloy heats is given in Table 3. These alloys were obtained as tubing stock from Century Tubes, Inc., and were used without further preparation, other than the machining and cleaning required for welding into the sample configuration.

Table 3. Composition of the alloys used in permeation tests.

Composition	Heat No.	Fe	Ni	Cr	Co	Mo	W	C	Al	
Incoloy 800H, 0.01 in. wall	V01283	46.65	30.84	19.76				0.06	0.37	Ti: 0.48; Si:0.49; Mn: 1.14; Cu: 0.07
Inconel 617, 0.01 in. wall	XX58A7UK	1.55	53.02	22.21	12.46	8.97		0.08	1.04	Ti: 0.29; Si:0.17; Mn: 0.07; Cu: 0.14

The samples tested had nominal 0.010 in. (0.254 mm) wall thicknesses. The diameter of the tube stock is 0.25 in. (6.35 mm). The actual wall thickness was determined by scanning electron microscopy (SEM) of radially sectioned and polished samples. The measured wall thickness for the samples is summarized in Table 4.

Table 4. Measured wall thickness of the as-received alloy tube stock.

	Wall Thickness (mm)		
Alloy	Nominal	Measured	Total Uncertainty (%)
Incoloy 800H	0.254	0.260	4.75
Inconel 617	0.254	0.257	4.46

The nominal sample configuration is shown in Figure 8, and consists of a 6-in.-long test section of Incoloy 800H or Inconel 617 tube welded to upper and lower thick-walled barrels of Inconel 600. The Inconel 600 tubes are 0.75 in. (19.1 mm) outer diameter and 0.25 in. (6.35 mm) inner diameter; the tubes were gun-drilled from round bar stock. The center portion of the thin-walled test section is the heated permeation zone. The thickness of the barrels and their location outside the heated zone ensure that they do not contribute measurably to the flux of permeating gas. The thick-walled barrel sections of the test sample are sealed by compression O-ring seals to the upper and lower mounting flange of the sample chamber.

The chemical and physical characteristics of the sample materials are described in detail in the hydrogen permeation study published at the end of FY-10 [11]. The work in 2012 used test specimen 21 (TS-21), which is Incoloy 800H with a 0.030 inch thick wall.

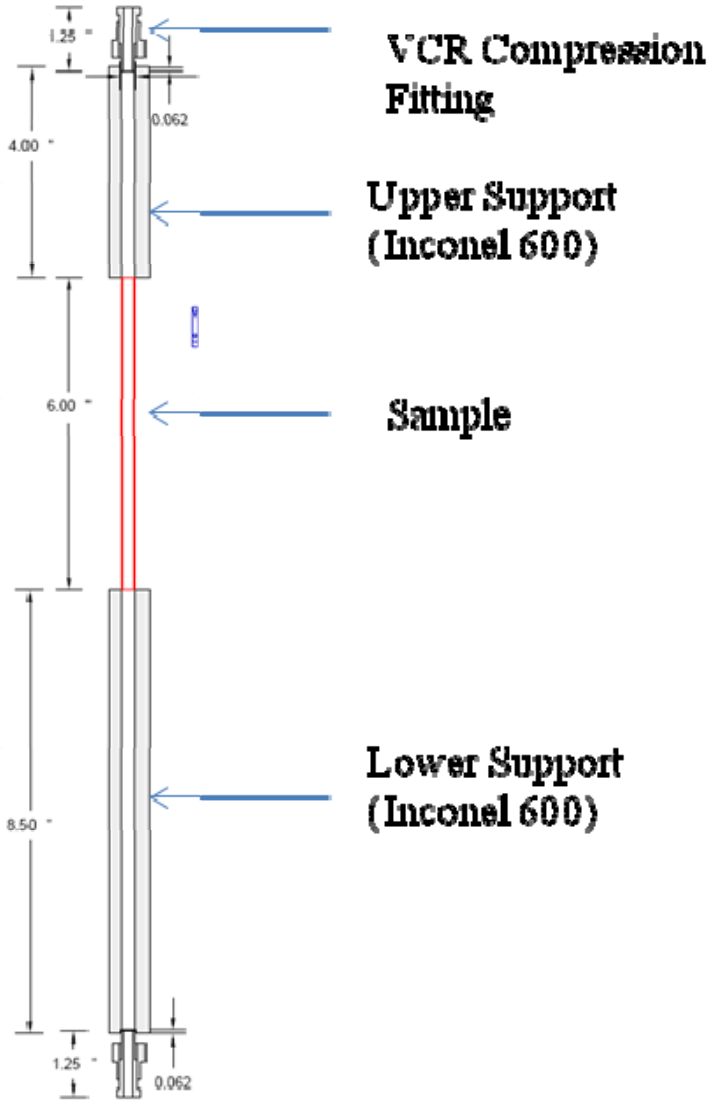

Figure 8. Configuration of the test sample.

3.3 Gas Mixtures

During the 2010 and 2011 experimental campaigns, tritium/helium gas mixtures were prepared in a two-step process. The first step used the Tritium Storage and Assay System (SAS) [also located in Safety and Tritium Applied Research Facility (STAR) facility] to fill an 11 cc cylinder with a known quantity of tritium. The 11 cc tritium cylinder is then removed from the SAS and connected to the permeation measurement system. The second step involves expanding the tritium into an evacuated volume and then backfilling the volume with ultra high purity (UHP) helium to obtain the desired tritium concentrations.

Tritium is stored in the SAS on two 47 g depleted uranium (DU) beds, each capable of holding 17,000 Ci of tritium. At room temperature, a DU bed getters all of the hydrogen isotopes. As the temperature of the DU bed is increased, the tritium partial pressure increases as a function of temperature and tritium is released from the DU bed. The SAS relies on pressure-volume-temperature measurements and a high purity tritium inventory to determine the quantity of tritium transferred to experiments. The following controls were used to ensure that the SAS accurately measures the quantity of tritium transferred.

1. The accuracy of the pressure sensors is verified annually against manometers whose calibrations are traceable to National Institute for Standards and Technology criteria.
2. Volumes were calibrated by filling a reference volume to a known pressure and then expanding the gas into an unknown volume at constant temperature. At least five repetitions of the expansion tests were conducted. Standard data reduction and analysis methods were used to determine the uncertainty associated with each volume. The reference volumes were certified by the Primary Standards Laboratory located at Sandia National Laboratories.
3. The SAS contains nine Omega Type-K thermocouples. For Omega Type-K thermocouples above 0ºC the error is 2.2ºC or 0.75% (whichever is greater).
4. Only high-purity tritium shipments are received into the SAS and DU bed to DU bed transfers are used to maintain the purity of the tritium inventory by removing ^{3}He decay products.

All tritium transfers are based on the ideal gas law and calculated using

$$A = (58023 \cdot X_T \cdot P \cdot V)/(R \cdot T) \quad (1)$$

where A (Ci) is the total activity, T_2 gas contains 58,023 Ci/mole, X_T is the tritium concentration ($X_T = 1$ following DU bed to DU bed transfers), and P (torr) is the pressure in volume V (cc) at temperature T (K). R (62,396 cc·torr/mole·K) is the universal gas constant.

The SAS provided 249 mCi of tritium in an 11.33 cc transfer volume for the Incoloy 800H permeation experiments and 250 mCi of tritium in an 11.35 cc transfer volume for the Inconel 617 permeation experiments.

Mixing the SAS-supplied tritium with commercial UHP helium to obtain the desired tritium concentrations takes place in a mixing manifold integral to the permeation measurement system. Components of the mixing manifold include two 1 L calibrated cylinders, a vacuum pump system, a 5,000 torr pressure sensor, a UHP helium supply gas cylinder, a mass flow controller, manual isolation valves, and ~15 cc of interconnecting tubing. The 11 cc tritium transfer volume is attached to the mixing manifold with a VCR coupling. The following steps were followed to prepare tritium/helium gas mixtures.

1. Evacuate the entire mixing manifold and then close all of the manual isolation valves.
2. Pressurize one of the 1 L cylinders to ~4,500 torr with UHP helium.
3. Expand the tritium in the transfer volume into the 15 cc of evacuated interconnecting tubing. Close the valve on the tritium transfer volume after 5 minutes.
4. Expand the tritium in the 15 cc of interconnecting tubing into the evacuated 1 L cylinder.
5. Expand the UHP helium in the 1 L cylinder into the 15 cc of interconnecting tubing and 1 L volume containing tritium. Allow the tritium and helium to mix at least overnight to ensure that a relatively consistent tritium concentration is achieved.

The tritium concentration was estimated using pressure-volume-temperature calculations and measured with an ion chamber. Due to nonuniform mixing, an estimated concentration was used for determining the operating concentration. This procedure creates a tritium/helium mixture large enough to verify the tritium concentration with an ion chamber and to run three permeation experiments. At the end of the three permeation experiments the mixing manifold was purged with UHP helium and evacuated. This mixing process was then repeated twice using the tritium remaining in the tritium transfer volume. In this way, primary gas loop of the system was supplied with a tritium/helium mixture at nominal concentrations of 6.0, 3.0, and 1.5 ppm.

Prior to the experiment sequence, the tritium concentration in the primary loop was measured using the ion chamber located in the ventilation hood. The following steps were followed to measure the tritium concentration in the mixture without heating of the test sample:

1. Pressurize the primary loop to 105 kPa with the T_2/He mixture.
2. Turn on the primary motor to circulate the mixture with 1 L per minute in the primary loop.
3. Open the primary output line and adjust the primary output leak valve to 15 sccm.
4. Measure the tritium concentration in the mixture via the 10 cc ion chamber in the ventilation hood.

Typically three experiments at 700, 800, 950°C (900°C for Alloy 617; all four in the second series of 800H testing) were performed with one tritium concentration except for one sequence of seven experiments using the 800H sample TS_20. (TS20-1 to TS20-7). Following the experiment sequence, this procedure was repeated to evaluate the tritium concentration in the primary loop. Figure 9 shows the ion chamber response during the tritium concentration determination procedure before and after the experiment sequence from TS17-4 through TS17-6. The red line denotes the ion chamber response before the experiment sequence, and the blue line denotes the post experiment value. t=0 denotes the beginning of the heating. The measured tritium concentrations before and after the experiment sequence are approximately 7.3 and 6.2 Ci/m^3, respectively. This discrepancy in the measured tritium concentration before and after the sequence might be due to the depletion of tritium in the primary during the sequence. These issues are discussed further in Section 4.1.

Mixtures for the 2012 tests were originally made for the Tritium Migration, Infiltration, and Scintillation Test (TMIST) program using SAS. The mixtures were made in large volume tanks that became available at the end of the TMIST test series. The tanks had been largely depleted during TMIST testing, but by repressurizing the tanks with UHP helium, it was possible to establish the desired mixtures at the working pressures necessary for operation in the VHTR tritium permeation testing, from ~0.5 to ~125 atom ppm tritium. The large volume tanks allowed extended test runs that were not possible using the 2 L mixed volumes that were used in the 2011 testing.

Following the tritium concentration determination in the primary loop, the secondary flow was initiated and the sample heated. The primary loop was operated with varying rates at which tritiated gas was bled to the exhaust duct. This is essentially identical to the procedure that was followed for the tritium permeability measurement with the previously reported hydrogen measurement [11]. The main difference in the test procedure is that the two ion chambers were used for the tritium detection instead of the quadrupole mass spectrometer for hydrogen detection.

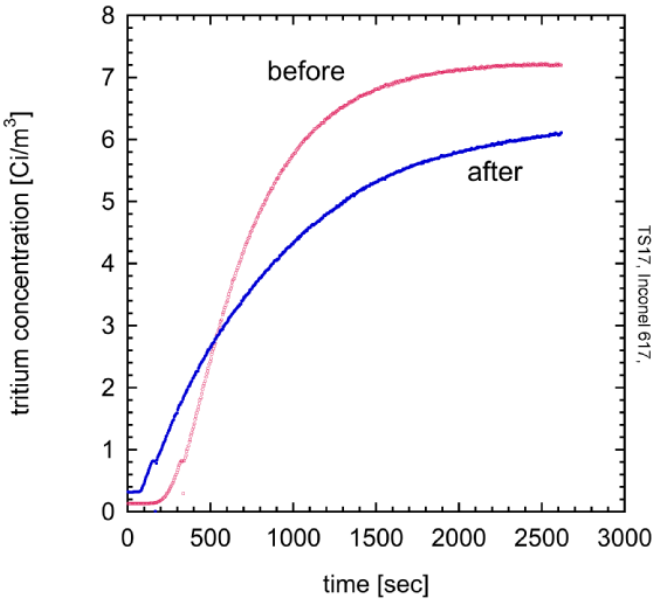

Figure 9. Ion chamber response of tritium concentration determination procedure before and after the experiment sequence from TS17-4 through TS17-6

3.4 Test Parameters

The gas permeability of materials depends on the sample temperature, the wall thickness and heated area of the sample, and the partial pressure of gas constituents on both sides of the sample. Permeability is affected by the oxidation state of the metal surface. The literature indicates that surface oxidation of these high Ni alloys can reduce the permeability by 2 to 3 orders of magnitude, consistent with the current test observations. The permeability is evaluated by measuring the flux of tritium molecules entering the secondary loop as a function the total volumetric helium flow rate in the secondary loop and the concentration of hydrogen in the helium flow. The following parameters were measured or controlled during the tests:

- Sample temperature and heated area, including the temperature distribution over the active heated area of the sample
- Concentration of tritium in the primary and secondary loops
- Concentration of hydrogen in the primary and secondary loops (measured in 2012 tritium test series only)
- Flow rate of helium in secondary loop input line
- Total pressure in primary and secondary loops.

The hydrogen permeability measurements were performed in the recirculation mode of operation. The permeation was measured with gas mixtures containing between 1.5, 3 and 6 ppmv T_2 in helium at a total pressure of 105 kPa for FY-11 tests. The measurements were made at peak sample temperatures of 700, 800, and 950°C. The tests were conducted on samples with 0.010 in. (0.254 mm) wall thickness. For Inconel 617, coupling of the radio frequency heater power to the 0.010 in. (2.54 mm) samples was insufficient to heat the 0.010-in.-thick samples above 900°C. Primary loop flow rates ranged from 2 to 15 standard cubic centimeters per minute (sccm), and secondary flow was 100 sccm.

In FY-12 testing, the composition was 0.5 and 125 atom ppm tritium in helium at a total pressure of 105 kPa, and the sample material was Incoloy 800H with a wall thickness of 0.030 in (0.762 mm).

Because residual background hydrogen had been identified as a potential influence on the tritium permeation, extensive bakeout and purging of the system with helium for multiple days was performed. This was determined to have minimal effect in reducing residual hydrogen and tritium values.

4. MEASUREMENT RESULTS

The permeability tests used tritium in helium in a recirculating mode at primary bleed rates of 2, 6 and 15 sccm. The gas in the loop is circulated by a bellows pump and exits the loop into the hood prior to discharge to the stack. In this mode of operation, the tritium in the primary loop may be depleted in modes at low rates of flow. In Figure 10, the blue trace represents the response of the 10 cc ion chamber monitoring the secondary tritium concentration along with the thermocouple temperature response. The red trace is the 1000 cc ion chamber, which has a slower response and a higher sensitivity. This configuration used both ion chambers in the tritium glovebox operating in series.

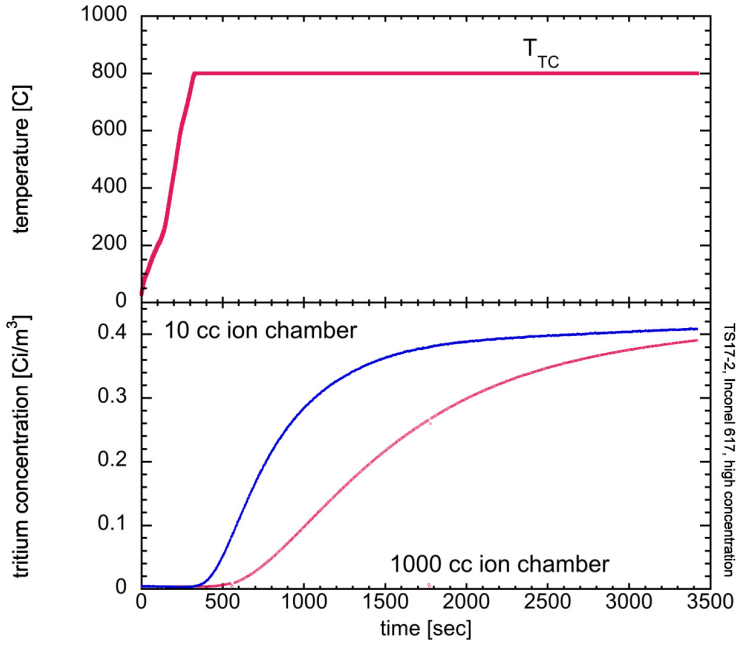

Figure 10. Temperature and Ion Chamber Response Test TS17-2, Inconel 617 at 800°C with gas flow 15 sccm. (2011 tests)

Permeability values are calculated assuming equilibrium conditions have been established. Despite performance of multiple tests on the sample at given concentrations, identification of this equilibrium was somewhat imprecise. In some cases, the test cycle was terminated due to the length of the working day rather than having achieved a definitive stable condition. This is seen in the following figures, from the TS21-9 test.

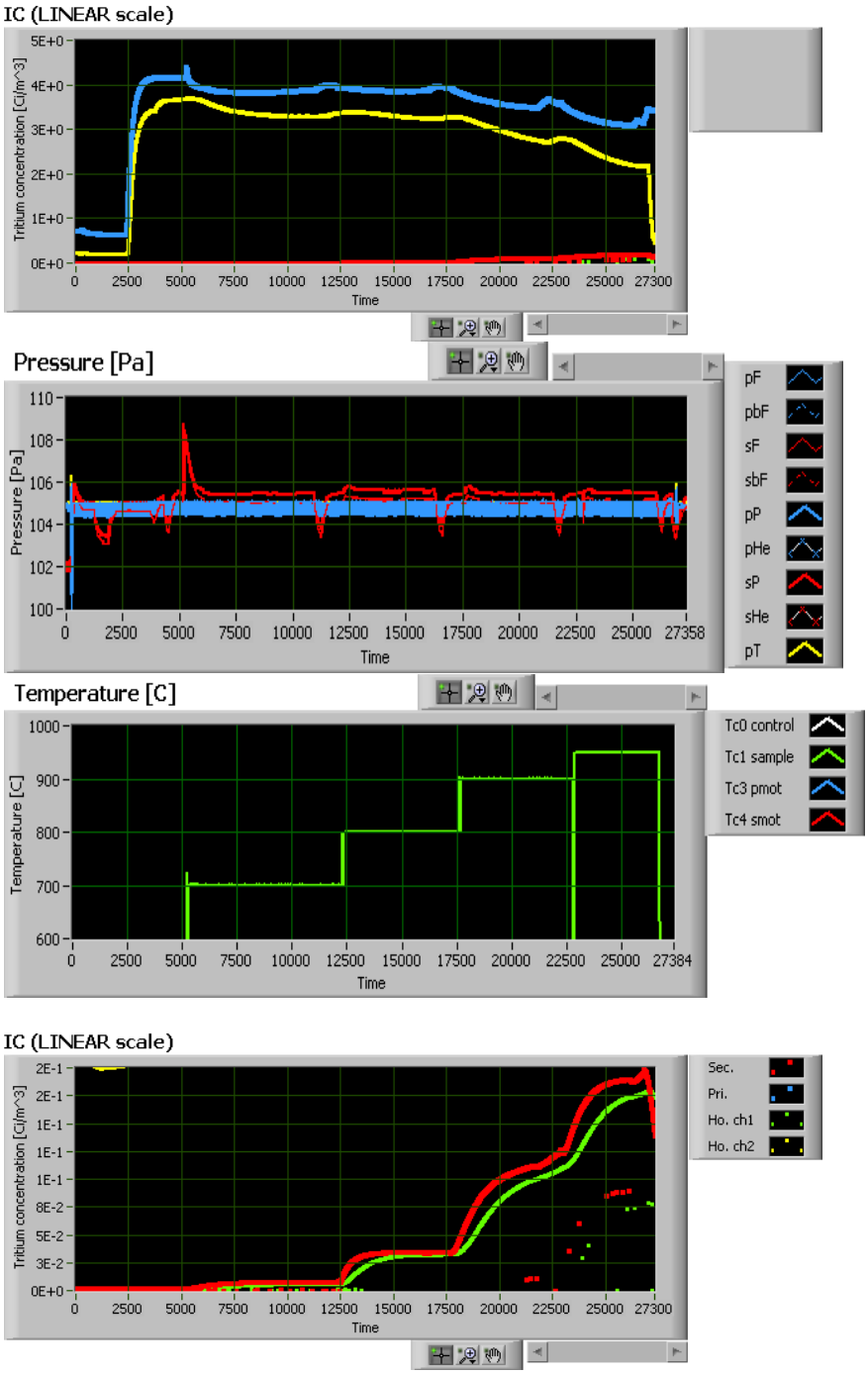

Figure 10a. FY-12 Test TS21-9 Process displays. Primary bleed flow 15.1 sccm, Secondary flow 100.1 sccm. At 950°C test termination, Primary loop: T_2= 3.18 Ci/m^3, H_2 concentration= 35.8 ppm Secondary loop: T_2= 194 mCi/m^3, H_2 concentration= 22.7 ppm.

In the top graphic, the red trace is the secondary loop tritium concentration as measured by the ion 1000 cc chamber located in the tritium permeation glovebox, and the green trace is the secondary loop tritium as measured by the second ion chamber located in the tritium recovery hood. The second graphic shows the blue trace as the primary loop tritium concentration as measured by the 10 cc ion chamber in

the glovebox and the yellow trace is the primary loop tritium bleed as measured by the ion chamber in the hood. Pulses or dips in the traces correlate to valving in the mass spectrometer to measure background, as noted on the red pressure trace in the third graphic. The fourth graphic shows the steps as the temperature was increased.

4.1 Diffusion Limited Permeation

Tritium molecules (T_2)[b] present in the primary helium flow dissociate at solid surfaces and permeate into the solid as individual atoms. Provided that diffusion through the solid is the rate limiting step in this process, the relation between T_2 partial pressure in the gas P_{T_2} and the T atom concentration C_T at the interface is given by Sieverts' law [15],

$$C_T = K_S \sqrt{P_{T_2}} \tag{1}$$

where K_s is the solubility, which has units ($1/m^3 \cdot Pa^{1/2}$) or ($1/cm^3 \cdot atm^{1/2}$). The T atoms in the metal diffuse through it according to Fick's law, which gives the constant flux J

$$J = -D\frac{\partial C_T}{\partial x} = D\frac{C_{T,1} - C_{T,2}}{x} \tag{2}$$

in terms of the primary side (subscript 1) and secondary side (subscript 2) T atom concentrations, the wall thickness x, and the diffusion coefficient D. Since Sieverts' law applies at both primary and secondary solid-gas interfaces, equations 1 and 2 can be combined to obtain the permeation model [4-5, 12, 16-18],

$$J_{T_2} = \frac{K\left(\sqrt{P_{T_2,1}} - \sqrt{P_{T_2,2}}\right)}{x} \tag{3}$$

where K is the permeability, the product of solubility and diffusivity ($K_s \cdot D$), which has units ($mol/m \cdot s \cdot Pa^{1/2}$) or (($cm^3$ T_2 @ STP)/($cm \cdot s \cdot atm^{1/2}$)). Note the definition of J_{T_2} in terms of molecules, though tritium diffuses as atoms through the solid.

Provided that pure helium enters the secondary inlet, the tritium activity detected in the secondary side is equal to the tritium mass flow due to permeation through sample

$$J_{T_2} A = C_{T_2,2} \dot{V}_{He,2} \tag{4}$$

where $C_{T_2,2}$ is the T_2 concentration in the secondary flow, $\dot{V}_{He,2}$ is the secondary helium flow rate, and A is the test section area through which permeation occurs. Combining Equations 3 and 4, the following expression for the permeability K is obtained:

$$K = \frac{C_{T_2,2} \dot{V}_{He,2} x}{A\left(\sqrt{P_{T_2,1}} - \sqrt{P_{T_2,2}}\right)}. \tag{5}$$

All quantities on the right hand side are known or measured in the experiment, so the permeability can be calculated for each data point with Eq. (5).

The permeability K is temperature dependent, and follows an Arrhenius law,

$$K = K_0 \exp\left(\frac{-Q}{RT}\right) \tag{6}$$

b We consider the implications of hydrogen, i.e. the presence of T_2 as well as HT, in subsequent sections.

where K_0 is the temperature-independent permeability constant, Q is the activation energy of permeation, R is the universal gas constant, and T is absolute temperature. A plot of the measured permeabilities vs. measured temperatures can be fit by Eq. (6) to determine the parameters K_0 and Q. However, this fitting is not straightforward for this particular experiment, because the temperature varied considerably along the test section. Thus, it is not obvious at which temperatures the measured permeabilities should be plotted. In a previous analysis of hydrogen permeation in this experiment, this issue was dealt with by fixing the temperature at the nominal (peak) value, and reducing the sample length (or equivalently, the permeation area) used to calculate permeation (Eq. (5)). The reduced length was based on engineering judgment.

Since the temperature distribution was measured and fit with a quadratic function as discussed in section 3.1, this function can be used to calculate the effective temperature. The full sample length L (6 in. or 15.24 cm) was used to calculate permeability from the experiment data. This permeability represents an average permeability $\overline{K}$ over the length of the sample and its range of temperatures. Since permeability is a function of temperature, and the temperature a function of sample length x ($0 \le x \le L$),

$$K(x) = K_0 \exp\left(\frac{-Q}{RT(x)}\right) \tag{7}$$

$T(x)$ has the quadratic form

$$T(x) = -Ax^2 + Bx + C \tag{8}$$

and the positive constants A, B, and C are determined from the IR camera data. Then the permeability may be written

$$K = K_0 \exp\left(\frac{-Q}{R\left(-Ax^2 + Bx + C\right)}\right). \tag{9}$$

The average permeability, $\overline{K}$, is simply the integral from $x = 0$ to $x = L$, divided by the total length L:

$$\overline{K} = \frac{1}{L}\int_0^L K_0 \exp\left(\frac{-Q}{R\left(-Ax^2 + Bx + C\right)}\right)dx \tag{10}$$

The parameters K_0 and Q were determined for the first 617 and 800H data by fitting a discretized form of the above integral equation to the measured permeation data with an iterative, non-linear least-squares procedure[c]. The variation of permeability along the sample length (Eq. (9)) is shown in Figures 11 and 13, and the Arrhenius plots displaying the experiment data, fit, and literature data are shown in Figures 12 and 14. In the Arrhenius plots, the measured permeabilities $\overline{K}$ from the experiment are plotted at the equivalent temperature $\overline{T}$, defined by

$$\overline{T} = \frac{-Q}{R\ln\left(\frac{\overline{K}}{K_0}\right)} \tag{11}$$

This is the temperature at which the permeability K (given by Eq. (6)) equals the measured average permeability $\overline{K}$, i.e. a permeability-weighted average temperature. The same concept has been employed in previous permeation experiments with variable temperatures [18]. A peculiar aspect of Eq. (11) is that the plotted *experiment* temperatures depend on the fit parameters; this is an inescapable consequence of

c Normally such a procedure would include a weighting of points based on their statistical error; lacking sufficient data, this weighting was not included.

making single permeation measurements over a range of temperatures, in which a functional relationship between K and T must be assumed.

The data collected in these initial permeability tests for both alloys are summarized in Appendices A and B.

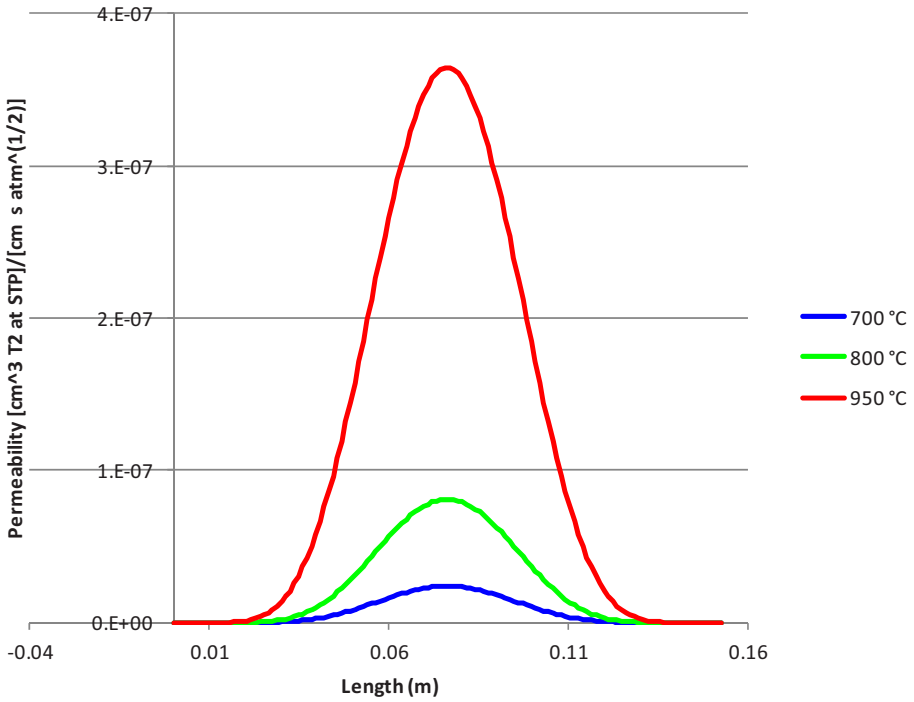

Figure 11. Calculated variation of Incoloy 800H permeability along the sample length.

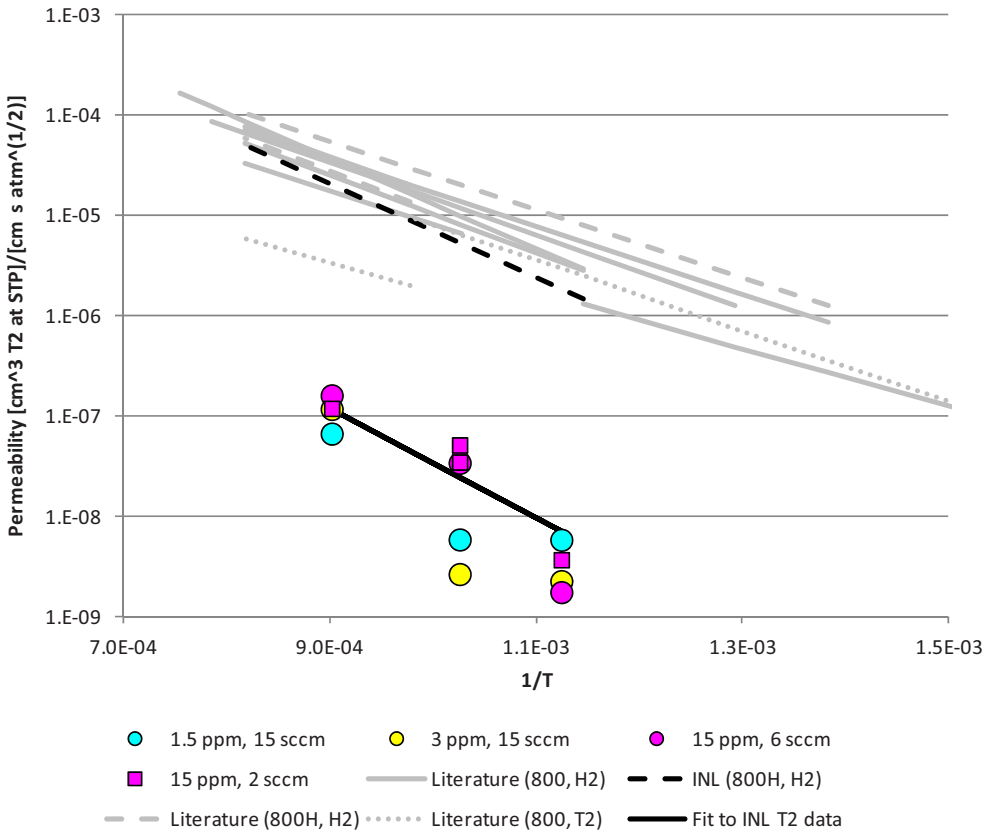

Figure 12. Arrhenius plot of Incoloy 800H tritium permeability (FY 11) with literature data.

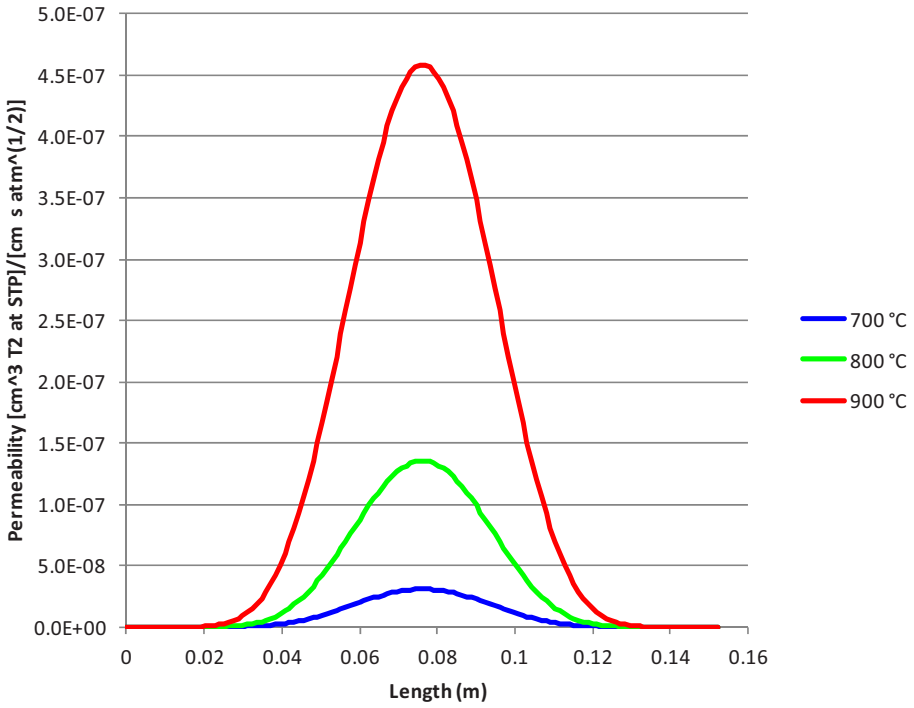

Figure 13. Calculated variation of Inconel 617 permeability along the sample length.

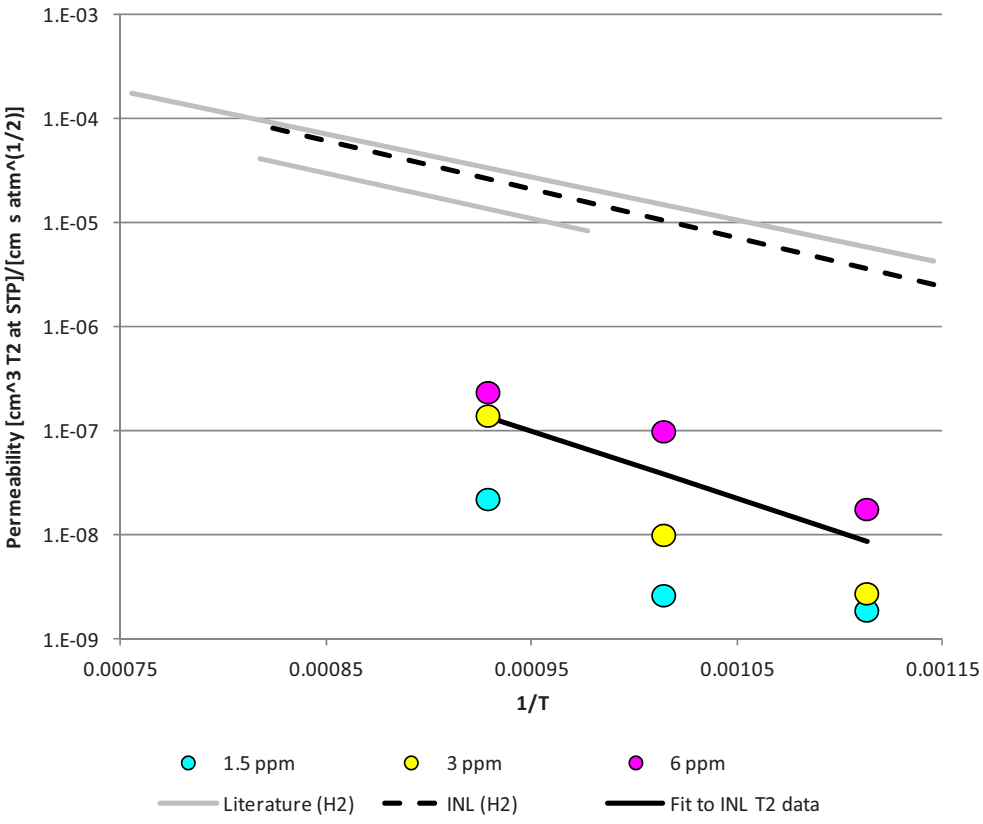

Figure 14. Arrhenius plot of Inconel 617 tritium permeability (FY 11) with literature data.

It is apparent from the figures that the calculated permeability for both alloys is much lower than has been reported in the literature. In the FY-11 testing several sources of uncertainty were identified that were suspected to have contributed to this. One was uncertainty in the primary tritium concentration; there was no dedicated ion chamber available to measure it during the tests. One of the secondary ion chambers was connected to the primary before each series of tests (fixed concentration at three different temperatures) to measure the initial primary concentration without heating (see section 3.3), then reconnected to the secondary side for the test series. This measured value was used in the calculation above, and it generally differed significantly from what was calculated for the initial gas mixture. It is suspected that tritium was being depleted over the course of each test series. To estimate this effect, the primary concentration was back-calculated from the measured secondary concentration and the value shown by the ion chamber located in the fume hood, which measures the combined primary and secondary exhaust. These adjusted values still gave a low permeability. The three sets of estimated primary concentrations are shown in Table 5.

Table 5. Primary tritium concentration determined by three different methods: 1) calculated based on the initial gas mixing; 2) measured once prior to each test series and assumed constant for the three temperature measurements in the series; 3) back-calculated from the fume hood exhaust.

		Tritium concentration (Ci/m^3)		
Material	Test ID	Method 1	Method 2	Method 3
Incoloy 800H	TS20_1	15.39	15.00	9.50
	TS20_2	15.39	15.00	4.99
	TS20_3	15.39	15.00	5.02
	TS20_4	15.39	15.00	5.18
	TS20_5	15.39	15.00	3.61
	TS20_6	15.39	15.00	4.66
	TS20_7	15.39	15.00	4.63
	TS20_8	3.06	7.80	5.97
	TS20_9	3.06	7.80	5.95
	TS20_10	3.06	7.80	4.08
	TS20_11	0.68	4.08	4.26
	TS20_12	0.68	4.08	4.39
	TS20_13	0.68	4.08	3.79
Inconel 617	TS17_1	35.89	15.54	10.04
	T170_2	35.89	15.54	9.57
	TS17_3	35.89	15.54	8.35
	TS17_4	7.46	7.31	5.15
	TS17_5	7.46	7.31	4.69
	TS17_6	7.46	7.31	3.36
	TS17_7	3.06	7.80	4.28
	TS17_8	3.06	7.80	4.24
	TS17_9	3.06	7.80	4.63

Another potential source of uncertainty was the likely presence of hydrogen. In the preceding analysis, it was tacitly assumed that tritium was the only hydrogen isotope present in the system. Measurements [11] during hydrogen-only testing found a persistent H_2 background of around 16 ppm.

Since this is on the order of and, in some cases, much larger than the primary T_2 concentration, it needs to be accounted for in the calculation; the dissociation and adsorption/desorption behavior at the surface is a chemical effect, which should not depend on the isotope.

Finally, it apparent that the effect is real, and that permeation deviates from square root dependence at the lower partial pressures. Such an effect is known to occur at low partial pressures in many metals due to dissociation at the surface, rather than diffusion through the bulk, limiting the permeation rate Some tests noted in the literature indicate that surface oxidation of high Ni alloys can reduce the permeability by 2 to 3 orders of magnitude, consistent with the current test observations. (cf. [20-25]). To investigate this, for FY-12 testing the system was modified to allow improved monitoring of both primary and secondary loops. This series of experiments was conducted with Incoloy 800H, at nominal partial pressures of 0.5, 5, and 125 ppma tritium. To eliminate the above-mentioned sources of uncertainty an additional ion chamber was configured to measure directly the primary concentration (see Figure 2a), and periodic checks of the hydrogen concentration were made with the quadrupole mass spectrometer (also pictured in Figure 2a).

Analysis of the new data requires a more general treatment of permeation, including multiple isotope effects; this theory and analysis is discussed in the next section.

4.2 General Permeation Analysis

Here we consider the more general case, in which there are two isotopes (H and T) and thus three distinct diatomic molecules (H_2, T_2, and HT) involved. Three transport processes are considered:
(1) dissociation of molecules in the gas, which become adsorbed atoms on the solid surface;
(2) recombination of surface atoms into diatomic molecules, which are released back into the gas; and
(3) diffusion of atoms through the solid layer. A schematic of these processes is shown in Figure 15; subscript 1 denotes the primary (“high” pressure side) and 2 the secondary side.

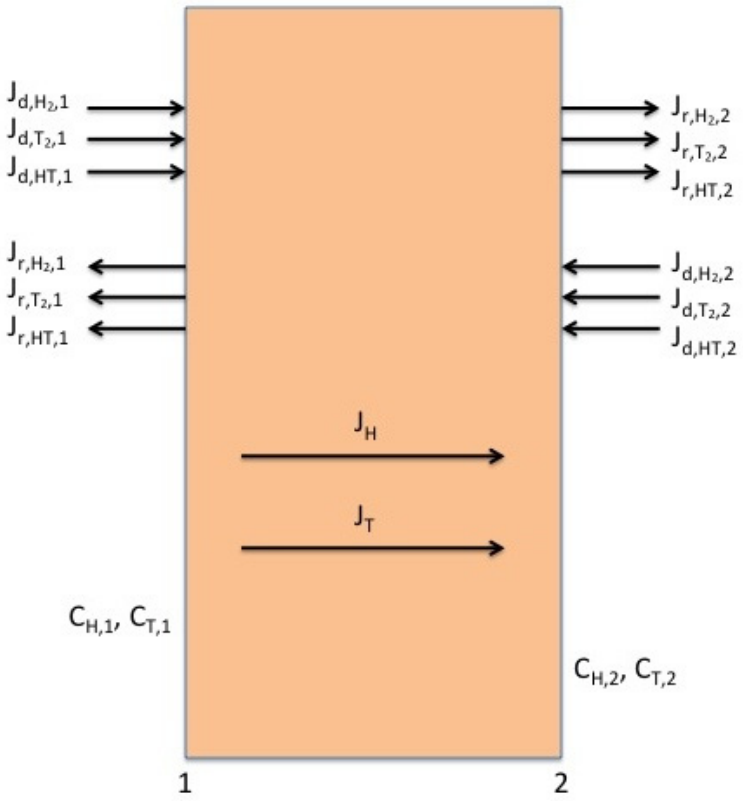

Figure 15. Schematic of surface dissociation and bulk transport processes occurring in the presence of hydrogen and tritium. Dissociation to, and recombination from, both primary and secondary sides occurs for all three molecular species. The difference is what diffuses through the barrier.

The dissociation flux is linearly dependent on the partial pressure of the given molecule, with constant of proportionality (dissociation rate coefficient) K_d:

$$J_{d,H_2} = K_d P_{H_2} \tag{12}$$

$$J_{d,T_2} = K_d P_{T_2} \tag{13}$$

$$J_{d,HT} = K_d P_{HT}\,. \tag{14}$$

Since two atoms are required, the recombination flux is proportional to the surface concentration of each atom (C_i) in the molecule, i.e.:

$$J_{r,H_2} = K_r C_H^2 \tag{15}$$

$$J_{r,T_2} = K_r C_T^2 \tag{16}$$

$$J_{r,HT} = 2K_r C_H C_T \tag{17}$$

where the constant of proportionality is the recombination rate coefficient, K_r. The fact that tritium atoms recombine just as readily with tritium or hydrogen atoms, if the latter are present, is reflected in Eq. (17), and this is why hydrogen concentrations can affect tritium permeation.

The dissociation and recombination described above is occurring on both primary and secondary surfaces. At “high” partial pressures, both the dissociation and recombination fluxes are large compared

to the diffusion flux. In other words, most atoms arriving via dissociation end up recombining and reentering the primary flow, and only a small fraction penetrate into the bulk. In this case, permeation to the secondary is limited by the bulk diffusion process and the surface concentrations can be obtained by setting the dissociation and recombination fluxes equal to each other:

$$K_d P_{H_2} = K_r C_H^2 \tag{18}$$

$$K_d P_{T_2} = K_r C_T^2 \tag{19}$$

$$K_d P_{HT} = 2K_r C_H C_T . \tag{20}$$

Note that we have tacitly assumed K_d and K_r are the same for hydrogen and tritium. In this case, equations 18-20 imply a relationship between the H_2, HT, and T_2 pressures:

$$P_{HT}^2 = 4P_{H_2} P_{T_2} . \tag{21}$$

This relationship is well satisfied at high temperature [19], so this assumption should be valid. Summing the three equations gives

$$K_d \left(P_{H_2} + P_{HT} + P_{T_2} \right) = K_r C_H^2 + 2K_r C_H C_T + K_r C_T^2 = K_r \left(C_H + C_T \right)^2 . \tag{22}$$

Rearranging leads to a two-isotope generalization of Sieverts' law:

$$C_H + C_T = K_S \sqrt{P_{H_2} + P_{HT} + P_{T_2}} \tag{23}$$

where Sieverts' constant K_s is given by the dissociation and recombination constants,

$$K_S = \sqrt{\frac{K_d}{K_r}} . \tag{24}$$

In the absence of hydrogen, Eq. (23) simplifies exactly to Eq. (1) for tritium (or vice versa). Thus, we see that Sieverts' law is a consequence of diffusion-limited permeation. In cases that are not strictly diffusion limited, the analysis described in Section 4.1 is not applicable, nor will a measurement of the permeating flux be proportional to the square root of pressure with constant of proportionality K, the permeability, where $K = K_s D$.

In the opposite extreme, permeation is surface-limited, i.e., limited by the rate of dissociation adsorption on the primary surface. In this case, diffusion through the bulk is the faster process, and the concentration profile across the solid is flat. Assuming the secondary pressure is effectively zero[d], i.e., the dissociation flux on the secondary side is negligible, then the permeating fluxes are simply equal to the recombination fluxes on the secondary side:

$$J_{H_2,2} = K_r C_{H,2}^2 \tag{25}$$

$$J_{T_2,2} = K_r C_{T,2}^2 \tag{26}$$

$$J_{HT,2} = 2K_r C_{H,2} C_{T,2} . \tag{27}$$

But since the concentration gradient is (near) zero across the solid,

d This assumption may not be well satisfied in this experiment, since significant hydrogen impurities were apparent in the secondary (see Table 6).

$$C_{H,1} = C_{H,2} = C_H \tag{28}$$

$$C_{T,1} = C_{T,2} = C_T \tag{29}$$

and thus, the same recombination flux must exist on the primary side. Since the fluxes on both sides must be equal,

$$K_d P_{H_2,1} - K_r C_H^2 = K_r C_H^2 \tag{30}$$

$$K_d P_{T_2,1} - K_r C_T^2 = K_r C_T^2 \tag{31}$$

$$K_d P_{HT,1} - 2K_r C_H C_T = 2K_r C_H C_T . \tag{32}$$

Combining equations 25/30, 26/31, and 27/32 gives:

$$J_{H_2,2} = \frac{1}{2} K_d P_{H_2,1} \tag{33}$$

$$J_{T_2,2} = \frac{1}{2} K_d P_{T_2,1} \tag{34}$$

$$J_{HT,2} = \frac{1}{2} K_d P_{HT,1} . \tag{35}$$

Unlike the diffusion-limited case, the above indicate that the flux is linearly dependent on partial pressure, and that in this surface-limited case the flux of each molecular species is independent of the others, i.e., the hydrogen pressure will not affect the tritium permeation as long as the hydrogen permeation is also surface-limited. This is only strictly true if H and T have the same K_d and K_s; where they differ the effect has been found to be small [20]. Though the ion chamber measurement of tritium concentration does not distinguish between T_2 and HT, an effective tritium flux and partial pressure can be defined that correspond directly to the detector measurements:

$$J_T = J_{HT} + 2J_{T_2} \tag{36}$$

$$P_T = P_{HT} + 2P_{T_2} . \tag{37}$$

Equations 34-37 imply

$$J_T = \frac{1}{2} K_d P_T . \tag{38}$$

Thus, if a plot of J_T vs. P_T is linear, this is confirmation of surface-limited permeation, and the slope of the line fixes K_d. This plot is shown for each of four temperature sets in Figure 16, along with power law fits to determine linearity.

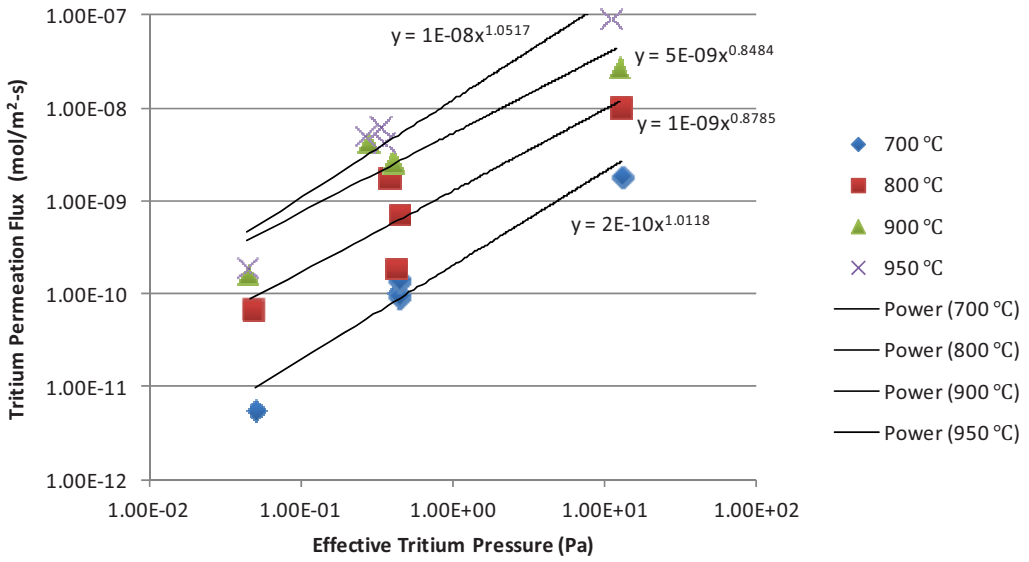

Figure 16. Tritium permeation flux versus effective tritium pressure (FY 12) at four different (peak) temperatures.

With only three data points on each line, it is difficult to draw any firm conclusions from Figure 16. There is clearly no square root dependence, but they are at best roughly linear, with exponents between 0.85 and 1.05. In each case (with the exception of one point at 800°C), the lowest and highest concentration points fall below the fit line, and the intermediate points above it. This is consistent with a slope change that would occur in the transition from surface-limited to diffusion-limited permeation. The slope between the intermediate (~5 ppma) and high (~125 ppma) points is between ½ and 1, consistent with such a transition; the slope between the low (~0.5 ppma) and intermediate (~5 ppma) points is actually higher than one. The low points here are particularly susceptible to errors, since these are on the order of background measurements that must be subtracted in calculating the flux, and also since some hydrogen dissociation occurring in the secondary would affect these points disproportionately. Though the approximate linearity of (at least portions of) the curve may be taken as preliminary evidence of the surface-limited regime, three pressures are clearly not sufficient to identify two slopes and a transition point, and because of this and the considerable scatter in the data points, a meaningful quantitative determination of K_d from this data is not possible. If the existence and range of the surface-limited regime can be more firmly established, K_d can be calculated from Eq. (38).

In the transition region and diffusion-limited regime, the tritium permeation is no longer independent of the amount of hydrogen present. In order to address this issue both the H_2 concentration and the tritium concentration were measured in the FY-12 series of tests. The ion chamber tritium measurement, however, does not distinguish between atoms bound in T_2 versus HT. Though in principle mass measurements could establish pressures of these two species, such measurements could not adequately resolve a T_2 signal, since the quantities involved are so small, and measurement of HT is not possible in this setup regardless of its partial pressure since it cannot be distinguished from the helium (He) carrier gas. However, if the equilibrium relation in Eq. (21) holds, the T_2 and HT partial pressures can be determined by solving Equations 21 and 37:

$$P_{T_2} = \frac{1}{2}\left[P_{H_2} + P_T - \sqrt{P_{H_2}\left(P_{H_2} + 2P_T\right)} \right] \tag{39}$$

$$P_{HT} = \sqrt{2\left[P_{H_2}^2 + P_T P_{H_2} - P_{H_2}\sqrt{P_{H_2}\left(P_{H_2} + 2P_T\right)} \right]}. \tag{40}$$

It is apparent that both of the above equations will be rather sensitive to the measured H_2 partial pressure when the amount of hydrogen in the system is comparable to, or larger than, the amount of tritium. As the hydrogen measurements summarized in Table 6 indicate, this was the case for all but the highest tritium concentrations measured in this test series.

Measurements of the H_2 concentration in the T_2/He bottles and during helium purge at low temperature indicate an apparent hydrogen concentration of a few ppm everywhere in the system, including the ultra-pure helium, and significantly higher (~15-25 ppm) concentrations in the primary loop upon heating, possibly a result of running up to 1% H_2 mixtures in prior experiment campaigns. Further scrutiny of these impurities indicates that the measurements of a few ppm must be in the detector noise, and are not adequately resolved. This is particularly evident in test TS21-9 from 700 to 800°C, where despite a temperature increase and a primary hydrogen concentration increase, the secondary hydrogen concentration *decreases*. A similar issue appears in test TS21-11, where measured secondary hydrogen concentrations at 700 to 800°C (and with increased primary hydrogen) are lower than during helium purge at low temperature. The background hydrogen in the secondary is particularly problematic for the analysis, since this must be subtracted when calculating the hydrogen flux (which in some cases is negative as noted above) but also because it may represent a non-negligible secondary pressure, which contributes a dissociation flux in the secondary and may prevent a truly surface-limited regime, even at arbitrarily low primary pressures. The existence of that regime is dependent upon the low secondary pressure assumption.

Table 6. Measured H_2 concentrations during tritium permeation testing.

	Primary	Secondary
Run ID	T_2/He H_2 conc. (ppm)	UHP He H_2 conc. (ppm)
3 ppm T_2/He	4.30	—
TS21-9 He purge	2.56	—
TS21-9 at 700 C	18.28	3.85
TS21-9 at 800 C	23.17	2.45
TS21-9 at 900 C	21.03	4.30
TS21-9 at 950 C	22.30	3.37
0.1 ppm T_2/He cylinder	1.15	—
TS21-10 He purge	2.73	1.65
TS21-10 at 22 C	3.56	1.20
TS21-10 at 700 C	15.76	2.05
TS21-10 at 800 C	15.44	2.40
TS21-10 at 900 C	15.74	3.68
TS21-10 at 950 C	14.98	3.11
100 ppm T_2/He cylinder	3.23	—
TS21-11 He purge	2.48	2.26
TS21-11 at 22 C	3.27	—
TS21-11 at 700 C	22.04	2.01
TS21-11 at 800 C	25.50	2.01
TS21-11 at 900 C	25.22	2.74
TS21-11 at 950 C	19.45	3.47

Note that UHP Helium may contain H_2 in concentrations up to 10 ppm as indicated by the BOC Gases specification sheet.

Provided that the secondary pressure of all isotopes in the secondary is small, the surface-limited regime is realizable, and the transition from surface-limited to diffusion-limited behavior is governed by a dimensionless number W. For a single isotope (say, hydrogen), W is given by [21]

$$W = \frac{K_d x \sqrt{P_{H_2,1}}}{K_s D} \tag{41}$$

where x is the sample thickness and all other parameters have been defined previously. $W<<1$ indicates surface-limited behavior, and $W>>1$ diffusion-limited behavior. An approximate[e] extension to the multiple isotope case can be given in light of Eq. (23) by

$$W = \frac{K_d x \sqrt{P_{H_2,1} + P_{HT,1} + P_{T_2,1}}}{K_s D} \tag{42}$$

.

An important implication of Eq. (42) is that the transition is determined by the square root of the sum pressure of all hydrogen isotopes, so it will generally be necessary to define or measure the hydrogen concentration in any model or experiment considering tritium permeation, unless it can otherwise be established that the ratio of hydrogen to tritium pressures is small.

e Approximate because of the fact that it assumes the diffusion coefficient, D, is the same for hydrogen and tritium. It is well established that for tritium D is lower by a factor of $\sqrt{3}$ (cf. [22]).

5. CONCLUSIONS

The design of the NGNP reactor and high-temperature components must consider the permeation of fission-generated tritium through the high-temperature components such as the heat exchanger. Loss of tritium represents an environmental release and/or contamination of the product hydrogen. To support engineering design, the tritium permeation of Incoloy 800H and Inconel 617 has been measured, and compared to test values established for these materials in hydrogen permeation.

A system was designed to emulate heat exchanger conditions for a helium-cooled high-temperature gas reactor. It was fabricated and tested for measuring the permeation of hydrogen and tritium through metal alloys at high temperatures. The system uses counter-flow gas loops with calibrated mass flow and pressure controllers, an induction heater to heat the tubular sample to temperatures in the range of 700 to 950°C, an ion chamber system for measuring tritium concentration in the loops, an internal calibrated thermocouple for controlling the sample temperature, and an infrared thermal imaging system for measuring the temperature distribution in the heated sample. The operation of the system was tested and validated using hydrogen in FY-10, tritium testing was first performed in FY-11, followed by tritium testing in FY-12.

The FY-11 series of measurements were analyzed using the same diffusion-limited permeation theory employed in previous hydrogen data analysis. The result was a permeability value that was approximately two orders of magnitude lower than previously measured for hydrogen. At the completion of these tests, however, it was not known if the effect was real. Though a transition from diffusion-limited to surface-limited permeation is known to occur in metals at low partial pressures [20-25] and might explain the lower values, there was some uncertainty about the measurements. Neither the primary loop tritium concentration nor the residual hydrogen concentrations were measured. The system was modified to directly measure these constituents, and in FY-12 a series of experiments was conducted using Incoloy 800H.

In order to interpret the results, a more general formulation of permeation theory has been given here that outlines the expected behavior at high and low partial pressures. Diffusion-limited permeation, in which the permeation flux is proportional to the square root of pressure, is expected at high pressures. The constant of proportionality is permeability, which is the product of solubility and diffusivity. At low pressures, surface-limited permeation is expected, in which case the flux is proportional to the pressure (the relationship is linear). The constant of proportionality in this case is $\frac{1}{2}K_d$, where K_d is the dissociation rate constant.

A dimensionless number, based on the square root of pressure, sample thickness, dissociation rate constant, and permeability, establishes what pressures qualify as high and low. In the presence of multiple isotopes, this number depends on the square root of the sum of all isotopes, thus the presence of hydrogen can shift the transition point for surface-limited tritium permeation. Though hydrogen alters tritium permeation in the transition region and in the diffusion-limited regime, it does not affect tritium permeation if both hydrogen and tritium are in the surface-limited regime. Thus, if the relationship between tritium flux and tritium pressure is linear, the surface-limited behavior is clearly established, and K_d can be obtained from the slope.

The new data set is presented in precisely this fashion. The flux clearly does not have a square root dependence on pressure, and is generally consistent with the linear relationship characteristic of surface-limited permeation, and may span some of the transition region between surface and diffusion limited permeation. A quantitative estimate of K_d could not be obtained because the data were taken at only three pressures, which was insufficient to clearly identify two regions with different slopes and the transition point between them. The tritium measurements also have a relatively high uncertainty that makes interpretation even more difficult. The same can be said of the hydrogen measurements, which were clearly at the limits of the detector resolution for this system, but are necessary to analyze tritium permeation outside the surface-limited regime.

In light of these results, several recommendations for subsequent tests can be made. First, an assessment of the high measurement uncertainties occurring in this system for both tritium and hydrogen needs to be performed. Provided the measurements can be refined, a subsequent test should include multiple points at lower tritium pressures, as this is necessary to firmly establish the surface-limited regime. The permeability of hydrogen (and thus also tritium) has already been determined at high partial pressures. Care should be taken to ensure subsequent data are not taken exclusively in the transition region, from which the relevant material constants cannot easily be obtained. Because it is a complicating factor, residual hydrogen concentrations should be minimized to the extent possible. This is particularly true for the secondary background hydrogen, which not only influences permeation but also obscures the determination of the hydrogen flux. A large secondary background will always serve to inhibit surface-limited behavior and cannot be accounted for in the theoretical framework described here. Since elimination of hydrogen to levels lower than tritium may never be realistic, a rigorous quantification of the hydrogen species present is desirable.

While an analytical determination of a permeability (or dissociation) constant cannot be readily made from the varied and complex data produced by this experiment series, loop tests performed by General Atomics as a part of their HTGR Fuels and Core Development program concluded that for tritium concentrations of $9x10^{-3}$ μCi/sccm, the tritium permeation rates are not significantly affected by the presence of hydrogen at less than 100 to 10,000 ppmv. For a tritium concentration of $8x10^{-5}$ μCi/sccm, the tritium permeation rate varies with temperature and hydrogen concentration, with less than a factor of 5 tritium permeation reduction in the temperature range from 300 to 500°C and hydrogen concentrations from a few hundred ppm to 21,000 ppm. At very low hydrogen concentrations where the effect of hydrogen on tritium permeation may be ignored, increasing the tritium concentration by a factor of 100 yielded an increase of tritium permeation rate by a factor of 20. In this case the variation of tritium permeation rate with tritium specific activity did not seem to obey either a linear relationship or a square root relationship [28]. Typical primary circuit tritium concentrations observed in Peach Bottom and Ft. St. Vrain reactors were $1\text{-}5x10^{-5}$ μCi/cm^3 [29].

The primary discussion of this revision addresses the idea that at very low concentrations of hydrogen isotopes, permeation through metals at high temperature appears to be linear with respect to hydrogen partial pressure, as has been alluded to in the literature for decades [24,25]. As mentioned by San Marchi, non-metals permeate linearly, which suggests that the surface oxide is the dominant barrier in this system at these temperatures and pressures. This result is consistent with the results seen by Takeda [27], in which there is identified a low pressure region in which it is presumed that chemisorption of molecular hydrogen into the oxide layer is the rate limiting step, followed by a transition zone, and at higher pressures, the expected lattice diffusion limited regime.

It is not known whether the present results are due to the presence of an oxide layer, or simply because of the very low partial pressures involved. Because the barrier membrane is a complex material composed of metallic and non-metallic barriers, experimental investigation is much more problematic than for a single component test. To better identify the phenomenon being observed, the characteristics of the membrane surface and the bulk material need to be known. At the test temperatures and high hydrogen concentrations, it is possible that the oxide (Cr_2O_3) layer on the candidate alloys has been chemically reduced to the point of compromise or complete removal. Changes in the surface oxide (primarily Cr_2O_3) and the composition of the metal may compromise the effectiveness of the barrier. Reaction of the chromia with the carbide in the steel to form carbon dioxide has been observed in long term elevated temperature tests at INL [26]. Mass 44 (CO_2) was detected in the primary gas stream in the permeation tests discussed here. Determination of oxide layer chemistry and integrity will be difficult, because the reformation of the oxide layer occurs in the presence of extremely low oxygen or water vapor conditions, so the sample would probably need to be transferred, mounted, and polished and in an inert environment.

6. REFERENCES

1. D. L. Hanson, *Test Plan for Characterizing Tritium Transport in a VHTR*, PC-000550-0, General Atomics, San Diego, CA, December 20, 2007.
2. Y. Mori, H. Ikegami, and T. Nakada, 1974, "49. High temperature helium heat exchange loop," *BNES Conference on the HTR and Process Applications, Institute of Civil Engineering, Westminster, London, November 26-28, 1974*, paper 49, pp 49.1-49.12.
3. K. Masui, H. Yoshida, and R. Watanabe, "Hydrogen Permeation through Iron, Nickel, and Heat Resisting Alloys at Elevated Temperatures," *Transactions of the Iron and Steel Institute of Japan*, Vol. 19, Issue 9, 1979, pp. 547-552.
4. H. D. Roehrig, R. Hecker, J. Blumensaat, and J. Schaefer, "50. Experimental facilities for the investigation of hydrogen and tritium permeation problems involved with steam methane reforming by nuclear process heat," *BNES Conference on the HTR and Process Applications, Institute of Civil Engineering, Westminster, London, November 26–28, 1974*, paper 49, pp 50.1-50.11. Also, H. D. Roehrig, R. Hecker, J. Blumensaat, and J. Schaefer, "Studies on the Permeation of Hydrogen and Tritium in Nuclear Process Heat Installations," *Nuclear Engineering and Design*, Vol. 34, 1975, pp. 157-167.
5. A. S. Schmidt, F. Verfuss, and E. Wicke, "Studies on the permeation of hydrogen and tritium through heat resistant alloys," *Journal of Nuclear Materials*, Vol. 131, Issues 2-3, 1985, pp. 247-260.
6. T. Tanabe, S. Imoto, and Y. Miyata, "Hydrogen Permeation through Incoloy 800," *Journal of Nuclear Science and Technology*, Vol. 16, Issue 4, 1979, pp. 310–302.
7. Y. Narita, "Study on Hydrogen Permeation through Super Alloys," *Proceedings of the Japan-U.S. Seminar on HTGR Safety Technology, Helium Technology Volume II*, BNL-NUREG-50689-Vol. II, Brookhaven National Laboratory, Upton, New York, September 15-16, 1977, pp. 71-85.
8. T. Tanabe, INTOR Study Group Report (IAEA 1979), EUR FU BRU/XII 501/79/EDV 80, 1974, cited by A. D. Le Claire, "Permeation of Gases Through Solids III-As Assessment of Measurements of the Steady State Permeability of H and its Isotopes through Ni and through Several High Ni Commercial Alloys and Steels," AERE-R-10846, United Kingdom Atomic Energy Authority Harwell, March 1983.
9. H. P. Buchkremer, H. J. Cordewiner, W. Diehl, G. Esser, D. Fischmann, R. Hecker, M. Hishida, J. Lambrecht, V. Malka, R. Raitz von Frentz, H. D. Roehrig, A. Tauber, and J. Schaefer, *Ueberblick ueber die neueren Arbeiten auf dem Gebiet des Wasserstoff- und Tritiumverhaltens in Hochtemperaturreaktoren*, Juel-1497, Kernforschungsanlage Juelich, GmbH, Contributions of the Institute of Reactor Development to the II Seminar on Hydrogen and Tritium Behavior in HTRs, March 8, 1978.
10. S. Bhattacharyya, E. J. Veserly, Jr., and V. L. Hill, *Determination of Hydrogen Permeability in Uncoated and Coated Superalloys, Interim Report*, DOE/NASA/0006-1, NASA CR-165209, prepared by Illinois Institute of Technology Research Institute, Chicago, IL, for the National Aeronautics and Space Administration, Lewis Research Center, January 1981.
11. P. Calderoni and M. A. Ebner, *Hydrogen Permeability of Incoloy 800H, Inconel 617, and Haynes 230 Alloys,* INL/EXT-10-19387, Idaho National Laboratory.
12. J. Schaefer, D. Stoever, and R. Hecker, "Terms and Results of Hydrogen Permeation Testing of Oxide-Scaled High-Temperature Alloys," *Nuclear Technology*, Vol. 66, 1984, pp. 537-549.
13. J. T. Bell, J. D. Redman, and H. F. Bittner, "Tritium Permeation through Clean Construction Alloys," *Journal of Materials for Energy Systems*, Vol. 1, 1979, pp. 55-59.

14. J. T. Bell, J. D. Redman, and H. F. Bittner, "Tritium Permeation through Clean Incoloy 800 and Sanicro 31 Alloys and through Steam Oxidized Incoloy 800," *Metallurgical Transactions A*, Vol. 11A, 1980, pp. 775-782.

15. A. Sieverts, "Über Lösungen von Gasen in Metallen," *Zeitschrift für Elektrochemie und angewandte physikalische Chemie,* Vol. 16, 1910, pp. 707-713.

16. R. A. Strehlow and H. C. Savage, "The Permeation of Hydrogen Isotopes through Structural Metals at Low Pressures and through Metals with Oxide Film Barriers," *Nuclear Technology*, Vol. 22, 1974, pp. 127-137.

17. W. M. Robertson, 1972, "Hydrogen Permeation, Diffusion and Solution in Pure Nickel and a Nickel Based Superalloy," *International Meeting on Hydrogen in Metals, Vol II, Kernforschungsanlage Juelich, Germany, March 20-24, 1972*, pp. 449-491.

18. G. R. Longhurst, G. A. Deis, P. Y. Hsu, L. G. Miller, and R. A. Causey, "Gamma Radiation Effects on Tritium Permeation Through Stainless Steel," *Nuclear Technology/Fusion,* Vol. 4, 1983, pp. 681-686.

19. C. San Marchi, B. P. Somerday, R. S. Larson, and S. F. Rice, "Solubility of hydrogen and its isotopes in metals from mixed gases," *Journal of Nuclear Materials*, Vol. 372, 2008, pp. 421-425.

20. K. Kizu, A. Pisarev, and T. Tanabe, "Co-permeation of deuterium and hydrogen through Pd," Journal of Nuclear Materials, Vol. 289, 2001, pp. 291-302.

21. I. Ali-Khan, K. J. Dietz, F. G. Waelbroeck, and P. Wienhold, "The rate of hydrogen release out of clean metallic surfaces," *Journal of Nuclear Materials*, Vol. 76/77, 1978, pp. 337-343.

22. A. S. Zarchy and R. C. Axtmann, "Tritium permeation through 304 stainless steel at ultra-low pressures," *Journal of Nuclear Materials*, Vol. 79, 1979, pp. 110-117.

23. H. K. Perkins and T. Noda, "Deuterium transport through 304 and 304L stainless steel at low driving pressures and 15 keV deuteron bombardment," *Journal of Nuclear Materials*, Vol. 71, 1978, pp. 349-364.

24. C. San Marchi, Technical Reference, Hydrogen Compatibility of Materials, Sandia National Laboratory.

25. R.M. Barrer, "The permeability of metal membranes to diatomic gases," *Philosophical Magazine* Series 7, Vol. 28, Issue 188, 1939, pp. 353-358.

26. F. Rouillard, C. Cabet, K. Wolski and M. Pijolat, "Oxide-Layer Formation and Stability on a Nickel-Base Alloy in Impure Helium at High Temperature," *Oxidation of Metals*, Vol. 68, 2007, pp. 133-148.

27. T. Takeda, J. Iwatsuki, and Y. Inagaki, "Permeability of hydrogen and deuterium of Hastelloy XR," *Journal of Nuclear Materials,* Vol. 326, 2004, pp. 47–58

28. "HTGR FUELS AND CORE DEVELOPMENT PROGRAM QUARTERLY PROGRESS REPORT FOR THE PERIOD ENDING AUGUST 31, 1975," General Atomics report GA-A13592, pp. 58-64.

29. R. D. Burnette and N. L. Baldwin, "Primary Coolant Chemistry of the Peach Bottom and Fort St. Vrain High Temperature Gas-Cooled Reactors," General Atomics report GA-A16163, November 1980.

Appendix A

Summary of Incoloy 800H Permeability Data

Appendix A

Summary of Incoloy 800H Permeability Data (FY-11)

A total of 13 permeability measurement tests were initially performed with Incoloy 800H. Parameters common to all tests include the sample thickness (0.0254 cm), sample length (15.24 cm), sample inner diameter (0.635 cm), primary and secondary helium pressures (105000 Pa), and secondary helium flow rate (100 sccm). Note that wherever the terms "lower" and "upper" appear, they refer to the sets of parameters that result in lower and upper bounds on permeability, not necessarily the parameters themselves.

Table A-1. Test parameters and tritium permeation data for Incoloy 800H.

			Primary Loop			Secondary Loop	
				T_2 Concentration, mol/m^3			
Test	Peak Temp °C	Average Temp °C	He flow rate sccm	Lower	Upper	T_2 Concentration, mol/m^3	T_2 Permeation Flow, mol/s
TS20_5	700	616	2	2.58E-04	6.22E-05	2.81E-07	4.52E-13
TS20_1	800	702	2	2.58E-04	1.64E-04	3.56E-06	5.72E-12
TS20_3	800	702	2	2.58E-04	8.65E-05	2.46E-06	3.96E-12
TS20_4	950	836	2	2.58E-04	8.92E-05	7.71E-06	1.24E-11
TS20_6	700	616	6	2.58E-04	8.02E-05	1.35E-07	2.17E-13
TS20_2	800	702	6	2.58E-04	8.59E-05	2.42E-06	3.89E-12
TS20_7	950	836	6	2.58E-04	7.98E-05	1.01E-05	1.62E-11
TS20_8	700	616	15	1.34E-04	1.03E-04	1.24E-07	2.00E-13
TS20_9	800	702	15	1.34E-04	1.03E-04	1.46E-07	2.35E-13
TS20_10	950	836	15	1.34E-04	7.03E-05	5.32E-06	8.55E-12
TS20_11	700	616	15	7.03E-05	7.34E-05	2.26E-07	3.63E-13
TS20_12	800	702	15	7.03E-05	7.57E-05	2.27E-07	3.66E-13
TS20_13	950	836	15	7.03E-05	6.53E-05	2.24E-06	3.60E-12

Table A-2. Tritium pressures for Incoloy 800H.

Test	Ave. Temp. °C	Primary T_2 Pressure, Pa		Secondary T_2 Pressure, Pa
		Lower	Upper	
TS20_5	616	6.45E-01	1.55E-01	7.00E-04
TS20_1	702	6.45E-01	4.08E-01	8.88E-03
TS20_3	702	6.45E-01	2.16E-01	6.14E-03
TS20_4	836	6.45E-01	2.22E-01	1.92E-02
TS20_6	616	6.45E-01	2.00E-01	3.37E-04
TS20_2	702	6.45E-01	2.14E-01	6.03E-03
TS20_7	836	6.45E-01	1.99E-01	2.52E-02
TS20_8	616	3.35E-01	2.57E-01	3.10E-04
TS20_9	702	3.35E-01	2.56E-01	3.64E-04
TS20_10	836	3.35E-01	1.75E-01	1.33E-02
TS20_11	616	1.75E-01	1.83E-01	5.63E-04
TS20_12	702	1.75E-01	1.89E-01	5.67E-04
TS20_13	836	1.75E-01	1.63E-01	5.59E-03

Appendix B

Summary of Inconel 617 Permeability Data

Appendix B

Summary of Inconel 617 Permeability Data (FY-11 only)

A total of nine permeability measurement tests were performed with Inconel 617. Parameters common to all tests include the sample thickness (0.0254 cm), sample length (15.24 cm), sample inner diameter (0.635 cm), primary and secondary helium pressures (105000 Pa), primary helium flow rate (15 sccm), and secondary helium flow rate (100 sccm). Note that wherever the terms "lower" and "upper" appear, these refer to the sets of parameters that result in lower and upper bounds on permeability, not necessarily the parameters themselves.

Table B-1. Test parameters and tritium permeation flow data for Inconel 617.

Test	Peak Temp °C	Average Temp °C	Primary Loop T_2 Concentration, mol/m^3 Lower	Primary Loop T_2 Concentration, mol/m^3 Upper	Secondary Loop T_2 Concentration, mol/m^3	Secondary Loop T_2 Permeation Flow, mol/s
TS17_1	700	625	2.68E-04	1.73E-04	1.33E-06	2.14E-12
TS17_2	800	713	2.68E-04	1.65E-04	6.74E-06	1.08E-11
TS17_3	900	804	2.68E-04	1.44E-04	1.46E-05	2.34E-11
TS17_4	700	625	1.26E-04	8.87E-05	1.47E-07	2.37E-13
TS17_5	800	713	1.26E-04	8.07E-05	5.19E-07	8.36E-13
TS17_6	900	804	1.26E-04	5.78E-05	6.06E-06	9.75E-12
TS17_7	700	625	2.58E-04	7.38E-05	1.46E-07	2.35E-13
TS17_8	800	713	1.34E-04	7.30E-05	1.46E-07	2.35E-13
TS17_9	900	804	1.34E-04	7.97E-05	1.15E-06	1.85E-12

Table B-2. Tritium pressures for Inconel 617.

Test	Ave. Temp. °C	Primary T_2 Pressure, Pa Lower	Primary T_2 Pressure, Pa Upper	Secondary T_2 Pressure, Pa
TS17_1	625	6.68E-01	4.32E-01	3.32E-03
TS17_2	713	6.68E-01	4.11E-01	1.68E-02
TS17_3	804	6.68E-01	3.59E-01	3.64E-02
TS17_4	625	3.14E-01	2.21E-01	3.67E-04
TS17_5	713	3.14E-01	2.01E-01	1.30E-03
TS17_6	804	3.14E-01	1.44E-01	1.51E-02
TS17_7	625	6.45E-01	1.84E-01	3.64E-04
TS17_8	713	3.35E-01	1.82E-01	3.64E-04
TS17_9	804	3.35E-01	1.99E-01	2.87E-03

Appendix C

Summary of Incoloy 800H Permeability Data (FY-12)

Appendix C

Summary of Incoloy 800H Permeability Data (FY-12)

A total of 20 permeability measurements were performed in the second series of Incoloy 800H tests. Parameters common to all tests include the sample thickness (0.0254 cm), sample length (15.24 cm), sample inner diameter (0.635 cm), primary and secondary helium pressures (105000 Pa), primary helium flow rate (15 sccm), and secondary helium flow rate (100 sccm).

Table C-1. Test parameters and tritium permeation flow data for Inconel 617.

Test	Peak Temp. °C	Measured Primary Tritium Ci/m^3	Measured Secondary Tritium Ci/m^3	Effective Primary Tritium Pressure Pa	Tritium Permeation Flux $mol/(m^2\ s)$
TS21_1	700	5.12E+00	5.36E-03	4.40E-01	9.75E-11
TS21_2	800	4.86E+00	1.08E-02	4.18E-01	1.96E-10
TS21_3	900	4.60E+00	1.50E-01	3.96E-01	2.73E-09
TS21_4	950	3.84E+00	3.65E-01	3.30E-01	6.65E-09
TS21_5	700	4.96E+00	7.26E-03	4.27E-01	1.06E-10
TS21_6	800	4.40E+00	1.03E-01	3.78E-01	1.85E-09
TS21_7	900	3.22E+00	2.47E-01	2.77E-01	4.47E-09
TS21_8	950	3.07E+00	2.92E-01	2.64E-01	5.27E-09
TS21_9	700	5.12E+00	1.05E-02	4.40E-01	1.45E-10
TS21_9	800	5.05E+00	4.46E-02	4.34E-01	7.67E-10
TS21_9	900	4.59E+00	1.57E-01	3.95E-01	2.82E-09
TS21_9	950	4.07E+00	2.48E-01	3.50E-01	4.48E-09
TS21_10	700	5.81E-01	1.96E-03	4.99E-02	5.83E-12
TS21_10	800	5.47E-01	5.42E-03	4.71E-02	6.90E-11
TS21_10	900	5.15E-01	1.11E-02	4.43E-02	1.73E-10
TS21_10	950	5.12E-01	1.28E-02	4.40E-02	2.03E-10
TS21_11	700	1.50E+02	1.07E-01	1.29E+01	1.93E-09
TS21_11	800	1.47E+02	5.81E-01	1.26E+01	1.06E-08
TS21_11	900	1.41E+02	1.61E+00	1.21E+01	2.94E-08
TS21_11	950	1.25E+02	5.28E+00	1.08E+01	9.63E-08